AD-A079 277 JOHNS HOPKINS UNIV BALTIMORE MD DEPT OF MECHANICS AN--ETC F/G 11/6
ULTRASONIC AND ACOUSTIC EMISSION DETECTION OF FATIGUE DAMAGE.(U)
JUL 79 S R BUXBAUM , S E FICK , R E GREEN F44620-76-C-0081
UNCLASSIFIED AFOSR-TR-79-1287 NL

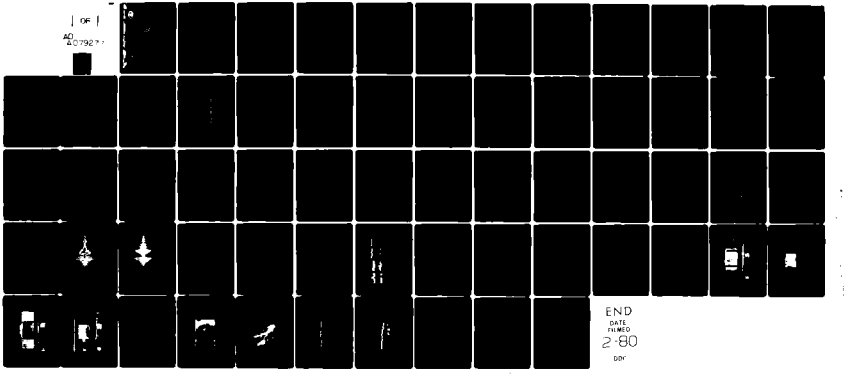

END
DATE FILMED
2-80
DDC

AFOSR-TR- 79-1287

AFOSR Scientific Report

5

THE JOHNS HOPKINS UNIVERSITY

Department of Mechanics and Materials Science

ULTRASONIC AND ACOUSTIC EMISSION DETECTION OF FATIGUE DAMAGE

by

S. R. Buxbaum
C. L. Friant
S. E. Fick
R. E. Green, Jr.

Air Force Office of Scientific Research

Contract No. F44620-76-C-0081

July 1979

Baltimore, Maryland 21218

Unclassified

SECURITY CLASSIFICATION OF THIS PAGE (When Data Entered)

REPORT DOCUMENTATION PAGE	READ INSTRUCTIONS BEFORE COMPLETING FORM
1. REPORT NUMBER (19) 18 AFOSR-TR-79-1287 ✓	2. GOVT ACCESSION NO. / 3. RECIPIENT'S CATALOG NUMBER
4. TITLE (and Subtitle) 6 ULTRASONIC AND ACOUSTIC EMISSION DETECTION OF FATIGUE DAMAGE,	5. TYPE OF REPORT & PERIOD COVERED INTERIM 1 June 1978 – 31 May 1979 / 6. PERFORMING ORG. REPORT NUMBER
7. AUTHOR(s) 10 S. B. BUXBAUM, C. L. FRIANT, S. E. Fick, R. E. GREEN, JR.	8. CONTRACT OR GRANT NUMBER(s) 15 F44620-76-C-0081 ✓
9. PERFORMING ORGANIZATION NAME AND ADDRESS JOHNS HOPKINS UNIVERSITY MECHANICS AND MATERIALS SCIENCE DEPARTMENT ✓ BALTIMORE, MD 21218	10. PROGRAM ELEMENT, PROJECT, TASK AREA & WORK UNIT NUMBERS 16 230[redacted] 11) E1 61102F
11. CONTROLLING OFFICE NAME AND ADDRESS AIR FORCE OFFICE OF SCIENTIFIC RESEARCH/NA BLDG 410 BOLLING AIR FORCE BASE, D C 20332	12. REPORT DATE 11) Jul[redacted]79 / 13. NUMBER OF PAGES 61
14. MONITORING AGENCY NAME & ADDRESS (if different from Controlling Office) 12) 64	15. SECURITY CLASS. (of this report) UNCLASSIFIED / 15a. DECLASSIFICATION/DOWNGRADING SCHEDULE

16. DISTRIBUTION STATEMENT (of this Report)

Approved for public release; distribution unlimited.

17. DISTRIBUTION STATEMENT (of the abstract entered in Block 20, if different from Report)

18. SUPPLEMENTARY NOTES

19. KEY WORDS (Continue on reverse side if necessary and identify by block number)

ULTRASONIC ATTENUATION
ACOUSTIC EMISSION
NONDESTRUCTIVE TESTING
FATIGUE
EDDY CURRENT
METALLOGRAPHY

20. ABSTRACT (Continue on reverse side if necessary and identify by block number)

The purpose of the present research is to optimize existing ultrasonic and acoustic emission techniques and to investigate new ones for early detection of fatigue damage in aluminum alloys used in aircraft construction. An ultrasonic pulse-echo system was used during fatigue cycling to record conventional A-scan wave forms as well as to monitor ultrasonic attenuation on 7075-T651 aluminum alloy specimens possessing different surface conditions. In addition, acoustic emission signals were recorded simultaneously with the ultrasonic measurements on each test specimen using two different acoustic emission systems. The task

DD FORM 1 JAN 73 1473

407 515

UNCLASSIFIED

SECURITY CLASSIFICATION OF THIS PAGE (When Data Entered)

of correlating evidence of cumulative fatigue damage and acoustic emission data was approached by the use of long term true-rms averaging of the system output and frequency domain analysis of acoustic emission signals recorded at selected intervals throughout the test. The integrity of the data was verified by independent electronic testing of the instrumentation, in situ eddy current and visual inspection, and metallographic examination.

5)

Ultrasonic and Acoustic Emission Detection of Fatigue Damage

ANNUAL TECHNICAL REPORT

(June 1, 1978 - May 31, 1979)

Air Force Office of Scientific Research

Contract No. F44620-76-C-0081

July 1979

Prepared by: S. R. Buxbaum, C. L. Friant, S. E. Fick, and R. E. Green, Jr.
The Johns Hopkins University
Baltimore, MD 21218

Submitted to: Lt. Col. J. D. Morgan, III
Air Force Office of Scientific Research/NA
Building 410
Bolling Air Force Base, D. C. 20332

Ultrasonic and Acoustic Emission Detection of Fatigue Damage

S. R. Buxbaum, C. L. Friant, S. E. Fick, and R. E. Green, Jr.
Department of Mechanics and Materials Science
The Johns Hopkins University
Baltimore, Maryland 21218

ABSTRACT

The purpose of the present research is to optimize existing ultrasonic and acoustic emission techniques and to investigate new ones for early detection of fatigue damage in aluminum alloys used in aircraft construction. An ultrasonic pulse-echo system was used during fatigue cycling to record conventional A-scan waveforms as well as to monitor ultrasonic attenuation on 7075-T651 aluminum alloy specimens possessing different surface conditions. In addition, acoustic emission signals were recorded simultaneously with the ultrasonic measurements on each test specimen using two different acoustic emission systems. The task of correlating evidence of cumulative fatigue damage and acoustic emission data was approached by the use of long term true-rms averaging of the system output and frequency domain analysis of acoustic emission signals recorded at selected intervals throughout the test. The integrity of the data was verified by independent electronic testing of the instrumentation, in situ eddy current and visual inspection, and metallographic examination.

INTRODUCTION

Various ultrasonic methods of detecting incipient fatigue damage in metals have been explored by the present investigators and their colleagues during the past several years. A summary of this research was published as Air Force Office of Scientific Research Report AFOSR-TR-76-0811 and reproduced by the Nondestructive Testing Information Analysis Center, NTIAC Newsletter Volume 5 No. 4 October 1977.

The purpose of the present research is to optimize current ultrasonic and acoustic emission techniques and to investigate new ones for the early detection of fatigue damage in aluminum alloys used in aircraft construction.

The extreme sensitivity of the nondestructive testing techniques of acoustic emission and ultrasonic attenuation to the microstructural alterations inherent in the mechanical deformation of metals has been well documented. These methods have been extensively exploited in basic research involving the fundamental mechanisms of plastic deformation, microcrack formation, crack growth, and fracture; they have also been widely used in technical investigations concerned with the detection of defects causing failure in structural materials. In theoretical treatments the experimental results obtained from both acoustic emission and ultrasonic attenuation measurements have been attributed to similar deformation mechanisms. Nevertheless,

the two techniques have seldom been used simultaneously in order to directly compare their advantages and disadvantages.

RESEARCH PROGRESS SUMMARY

In the present work acoustic emission monitoring and ultrasonic attenuation monitoring were compared as indicators of microstructural alterations during mechanical deformation. 7075 aluminum was chosen as test material because of the existence of published opinions of other investigators as to the origin of the observed acoustic emission signals. The results of prior investigators indicate that, for the aluminum alloy under study, the deformation mechanisms underlying acoustic emission are different from those causing changes in ultrasonic attenuation. This suggests that the two monitoring techniques can be synergistically combined, thereby synthesizing a method yielding far more information than either technique alone.

In previous work, simultaneous acoustic emission and ultrasonic attenuation monitoring was conducted during tensile elongation of test specimens of 7075 and several other aluminum alloys, as well as during fatigue testing of prismatic bars of 7075-T651 aluminum. In performing the present research, efforts were made to improve upon and to extend the previous work to more realistically simulate typical in-service conditions by conducting fatigue tests at lower stresses and therefore for longer time periods. Some tests were terminated prior to fracture after the occurrence of significant

changes in acoustic emission or ultrasonic attenuation were detected. In these cases eddy current scanning was then used to locate the crack responsible for the observed changes. Metallographic examination of the crack initiation region was performed in order to investigate the relationship between the observed features of the ultrasonic data and the physically deformed microstructure. The acoustic emission system used in earlier work was supplemented by a second system of different type, which permitted comparison of signal processing techniques. Improved instrumentation was used to obtain long-term averages of the acoustic emission signal energy and to record individual burst waveforms for later analysis both in the time and frequency domains. This facilitated discrimination among emissions caused by defect initiation, defect growth, and extraneous mechanical noise. The specimens were subjected to several different surface preparations in order to assess the effect of surface condition on the early detection of fatigue damage using acoustic emission and ultrasonic attenuation techniques. The prismatic bar shape used previously was modified so as to permit simultaneous ultrasonic attenuation and dual acoustic emission measurements to be made in combination with in situ eddy current and visual inspection. The new specimen geometry and mounting arrangement is shown in Fig. 1. Extraneous machine noise was decoupled from the specimen by placing 1/16 in. thick Teflon pads on all surfaces of contact between the specimen and the fatigue machine grips. As shown, the acoustic emission transducers were mounted on the upper and lower

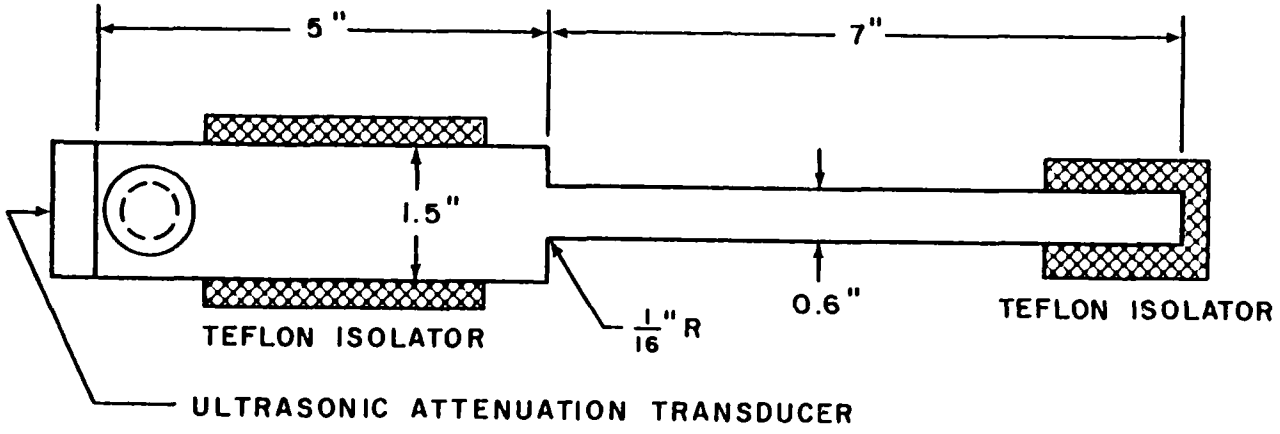

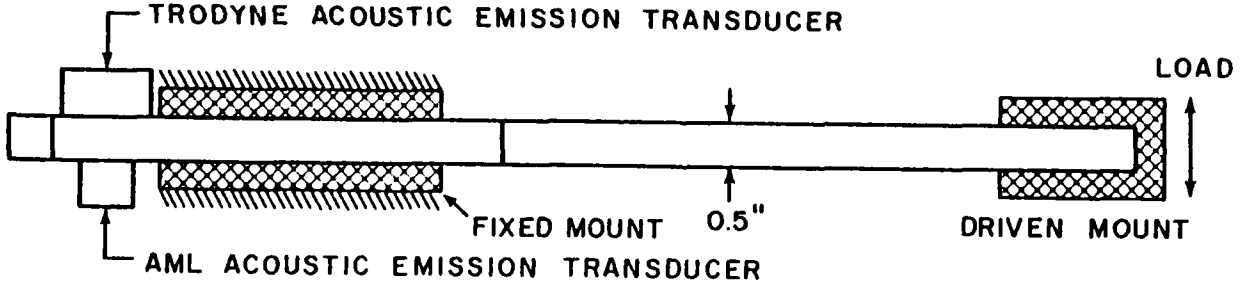

FIGURE 1. TOP AND SIDE VIEW OF FATIGUE TEST SPECIMEN

surfaces of the test specimens between the fixed grip and the end-mounted ultrasonic attenuation transducer. A sharp reduction in cross-section was machined in each specimen in order to provide a stress concentration region and thus localize the region of probable failure. This localization simplified the visual and eddy current examination for surface breaking cracks during fatigue cycling. The shoulder of the reduced cross-section was located sufficiently far from the fixed steel grip that any deleterious effects on eddy current testing that would otherwise be caused by close proximity were eliminated. The constricted area also ensured that the radiated sound field of the transducer overfilled the region where fatigue damage occurred. As shown in Fig. 1, the corners formed at the reduced cross-section incorporated a 1/16 in. radius in order to eliminate erratic experimental results caused by notches introduced by machining of square corners.

The fatigue machine; acoustic emission, ultrasonic attenuation, and eddy current instrumentation; and the specimen mounting arrangement are illustrated schematically in Fig. 2. The fatigue machine causes the test specimen to be loaded in reverse bending as a cantilever beam at a rate of 1725 cycles per minute. Stepless adjustment of an eccentric cam permits variation of the beam deflection over a wide range of values.

Two different commercial systems incorporating different transducers were used to obtain acoustic emission data. This allowed

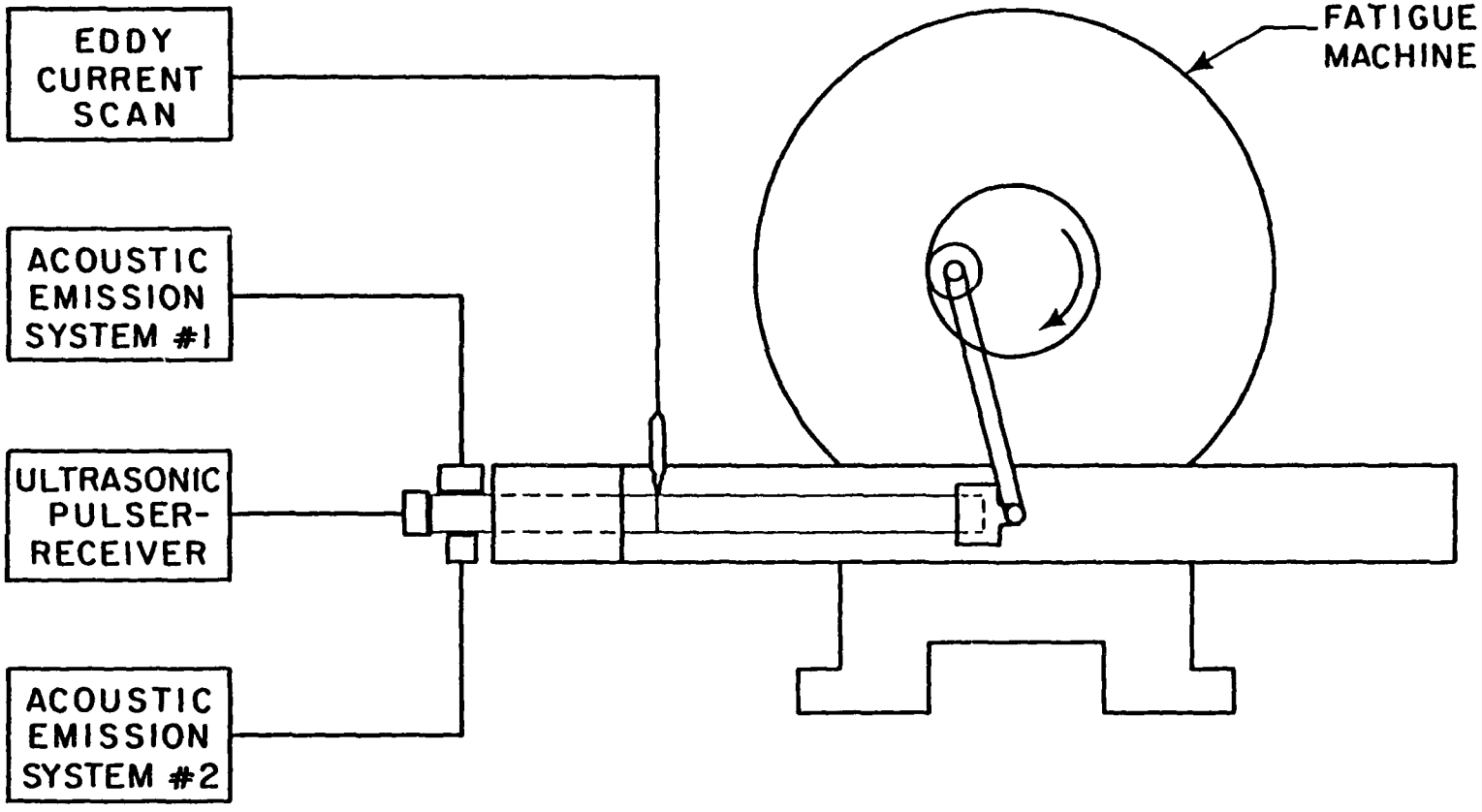

FIGURE 2. FATIGUE TEST APPARATUS AND SPECIMEN MOUNTING ARRANGEMENT

comparisons of the systems to be made both on the electronics test bench and under actual operating conditions. The use of tandem systems provided a safeguard against complete loss of data in the event of equipment failure and allowed simultaneous comparison of different strategies of analog signal processing using the same data. A schematic of the combined ultrasonic attenuation and acoustic emission monitoring systems is shown in Fig. 3. Attenuation data was recorded in two forms. A multipoint strip-chart recorder was used to obtain a continuous record of the attenuation as the scaled logarithm of the ratio of the amplitudes of two selected echoes. In addition, the pulse-echo pattern displayed on the monitor oscilloscope was photographed at intervals throughout the test. Two methods were also employed for monitoring acoustic emission. A digital oscilloscope (Nicolet Explorer III) was used at propitious times during the tests to record individual burst waveforms from both acoustic emission systems simultaneously. A floppy disc memory allowed later computer processing of the data. Since burst waveform data is sufficiently information-intensive to preclude its continuous long-term recording, true-rms voltmeters were used at the analog outputs of the acoustic emission systems in order to integrate the data during the course of an experiment. The averaged outputs of the voltmeters were continuously recorded on the strip-chart recorder.

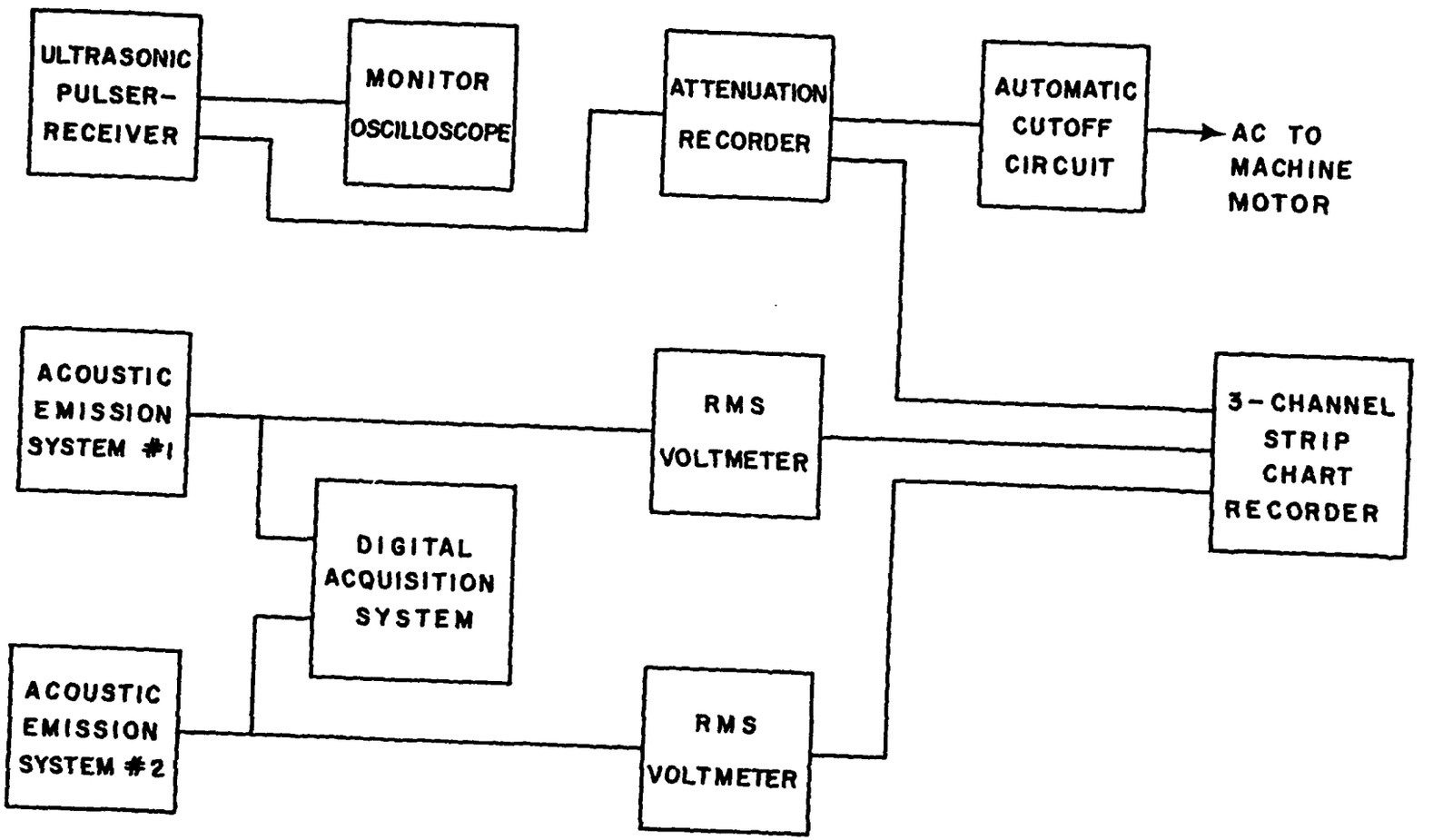

FIGURE 3. ULTRASONIC ATTENUATION AND ACOUSTIC EMISSION MONITORING SYSTEMS

Ultrasonic Attenuation System

The ultrasonic attenuation system is composed of a Matec 6600 pulser-receiver, with a 950B rf plug-in, and a 2470A attenuation recorder. An Aerotech Gamma Series 10MHz longitudinal mode transducer with a ½ by 1 in. active area was used with the ultrasonic system. The attenuation recorder includes a time gate permitting selection of any two echoes from the received wave train, automatic gain control to stabilize the amplitude of the echoes, and circuitry to obtain the logarithm of the ratio of the two selected echo amplitudes. The attenuation recorder was modified to allow the selection of the leading echo as either the numerator or denominator in the log ratio. This feature was introduced in order to obtain enhanced sensitivity to fatigue damage for certain attenuation measurement schemes. The rf pulses applied to the specimen were synchronized with the fatigue loading cycle by the use of an optical pickup from the rotating shaft of the fatigue machine. This assured consistency in the recorded data by avoiding beat frequency effects associated with random pulsing. A variable delay interposed between the optical trigger and the sync input of the pulser-receiver allowed attenuation to be measured at any desired point in the load cycle. A typical pulse-echo pattern is shown in Fig. 4. Peak A is due to the reflection of ultrasonic energy from the reduced cross-section shoulder of the specimen. The next large echo, peak C, is due to reflection from the end of the specimen.

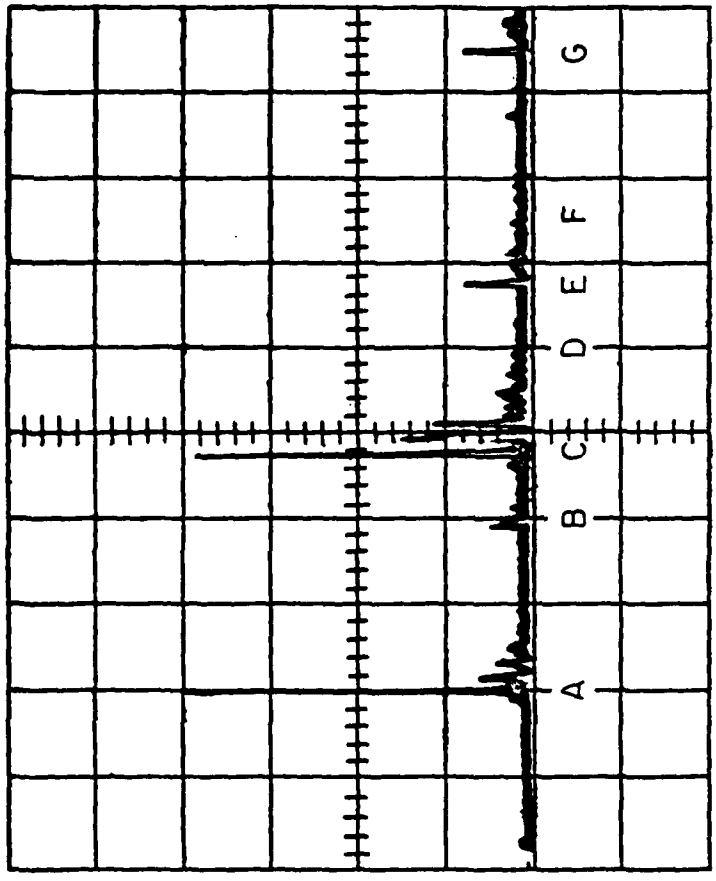

FIGURE 4. TYPICAL PULSE-ECHO PATTERN WITH SIGNIFICANT PEAKS LETTERED

The other labeled echoes in Fig. 4 will be discussed later in an analysis of the effectiveness of ultrasonic attenuation measurements as indicators of crack initiation. The attenuation recorder was adjusted to utilize echoes A and C because experimentation revealed that other usable pairs of echoes gave attenuation values less sensitive to fatigue damage. The continuous record of attenuation, plotted on a Leeds and Northrup 250 Series multipoint recorder, was used for trend analysis, while the oscilloscope photographs of the pulse-echo pattern were used for verification and to check for gross abnormal damage in the specimen.

The operational difficulties associated with the occurrence of significant events when a fatigue test was unattended were avoided by the use of electronic devices to automatically halt the test. One device monitored the rate of rise of the attenuation and triggered when a pre-set threshold was exceeded. This circuit was designed to be completely insensitive to slow signal drift caused by any part of the experimental apparatus. Since this device was unresponsive to changes approximately 8 percent of the time, i.e., tripping might be delayed 5 sec. with an 0.08 probability, a second unit was designed to trip instantly if the attenuation deviated from a range bounded by two set points. This device was used when the need for rapid response outweighed the inconvenience of false alarms. The use of automatic cutoff circuitry allowed inspection of the specimen at selected increments of attenuation change and thereby correlation of specimen surface damage and the attenuation data, with minimal

down time and relaxation effects.

Acoustic Emission Systems

The acoustic emission systems used in this research were an AML Type 3 Acoustic Emission Amplifier, loaned by the Admiralty Materials Laboratory (now the Admiralty Marine Technology Establishment) and a Trodyne Model 7500-4 Acoustic Emission Source Location System. Since the experiments performed during the course of this research did not involve event counting, the independent proof of performance tests conducted with the instruments were limited to the analog circuitry. Frequency response was measured both for the amplifier sections alone and for the complete systems including transducers. The amplifier section tests were made using a Hewlett Packard 310A Wave Analyzer to drive the amplifier input through a suitable termination. The frequency response of a complete system was measured by driving the transducer attached to it with an acoustical signal generated by a second transducer excited by the wave analyzer. The frequency response of this second transducer was independently measured with driving and driven transducers acoustically coupled. The output broadband noise voltage with no input voltage applied, i.e., the noise floor, of each system was measured with the Fluke 8920A true-rms voltmeters used to measure the acoustic emission levels during fatigue tests. The transducers were electrically connected but acoustically isolated for the noise floor tests.

The AML system was the less complicated of the two acoustic emission systems used. Its significant features include extensive

electrical shielding and provision for battery operation to avoid powerline-induced disturbances. The transducers supplied with the unit consisted of a small cube of PZT-8 mounted in a brass housing containing a rf matching transformer. A multi-shielded Mu-metal and copper screened cable was provided to carry the low level acoustic emission input signal to an 18 dB preamplifier contained in the main amplifier cabinet. The electrical frequency response of the main amplifier at 70 dB gain is shown in Fig. 5. The bandwidth is constant over the available gains of 60-100 dB since the gain is increased by switching in additional 10 dB stages. The frequency response of the complete system is shown in Fig. 6. It can be seen that the bandwidth is reduced and modulated by transducer resonances. A plot of driving transducer terminal voltage versus frequency, Fig. 7, with the transducer excited by a high impedance rf generator, shows that the additional resonances are in the driven Admiralty transducer. The rms noise floor voltage, over a bandwidth of 20 MHz, varied from 2.6 mV at 60 dB gain to 210 mV at 100 dB gain, which is consistent with the design of the unit. Since the maximum rms voltage swing at the analog output jack is 1 volt, the available dynamic range varies from 30 dB at 60 dB gain to 14 dB at 100 dB gain. Although the available dynamic range is completely adequate for event counting, care was necessary in these evaluation experiments to maintain sufficient gain while avoiding overload.

The Trodyne system utilized a small 10 dB preamplifier module to minimize the effects of the coaxial cable connecting the transducer

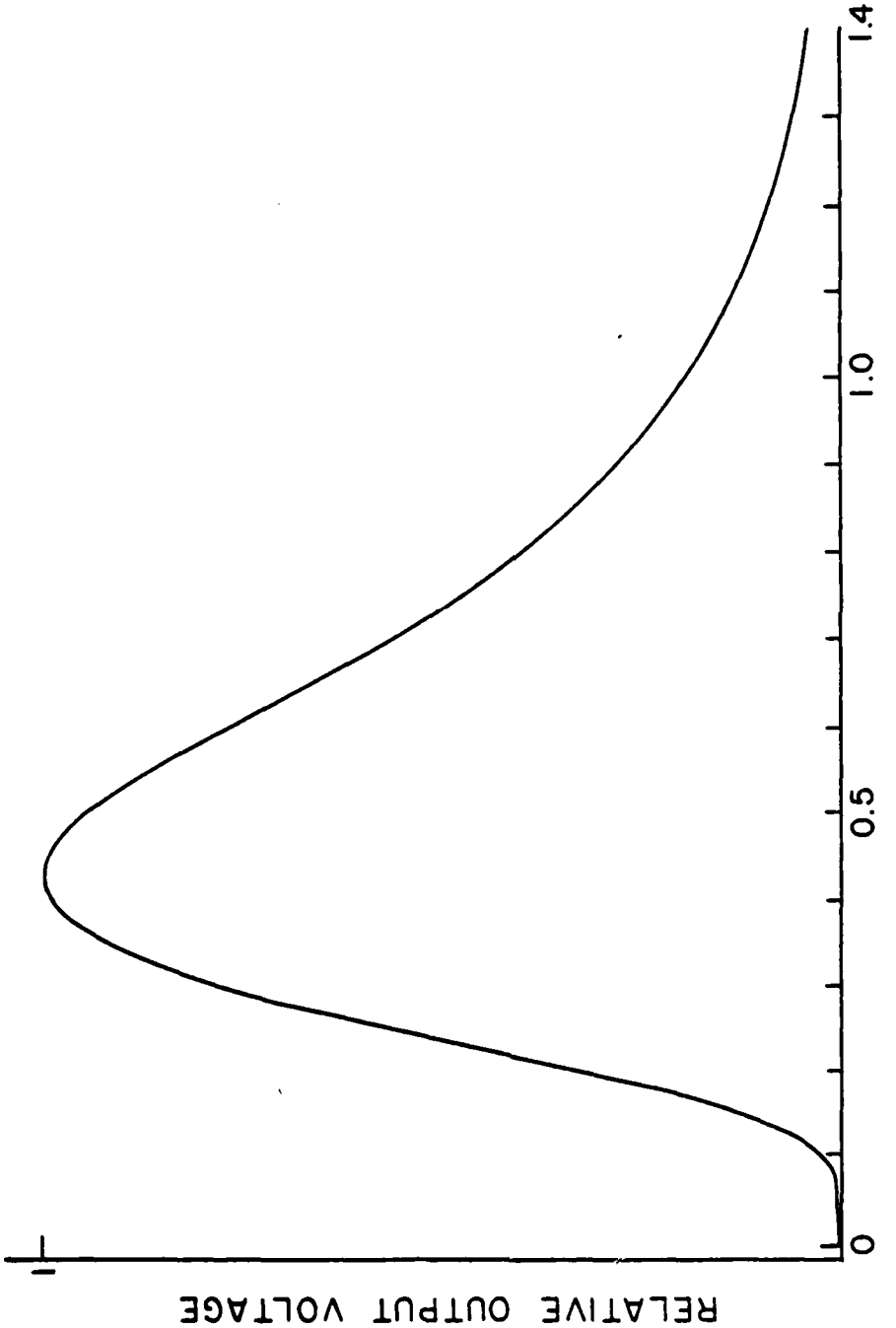

FIGURE 5. FREQUENCY RESPONSE OF ADMIRALTY AE SYSTEM AMPLIFIER

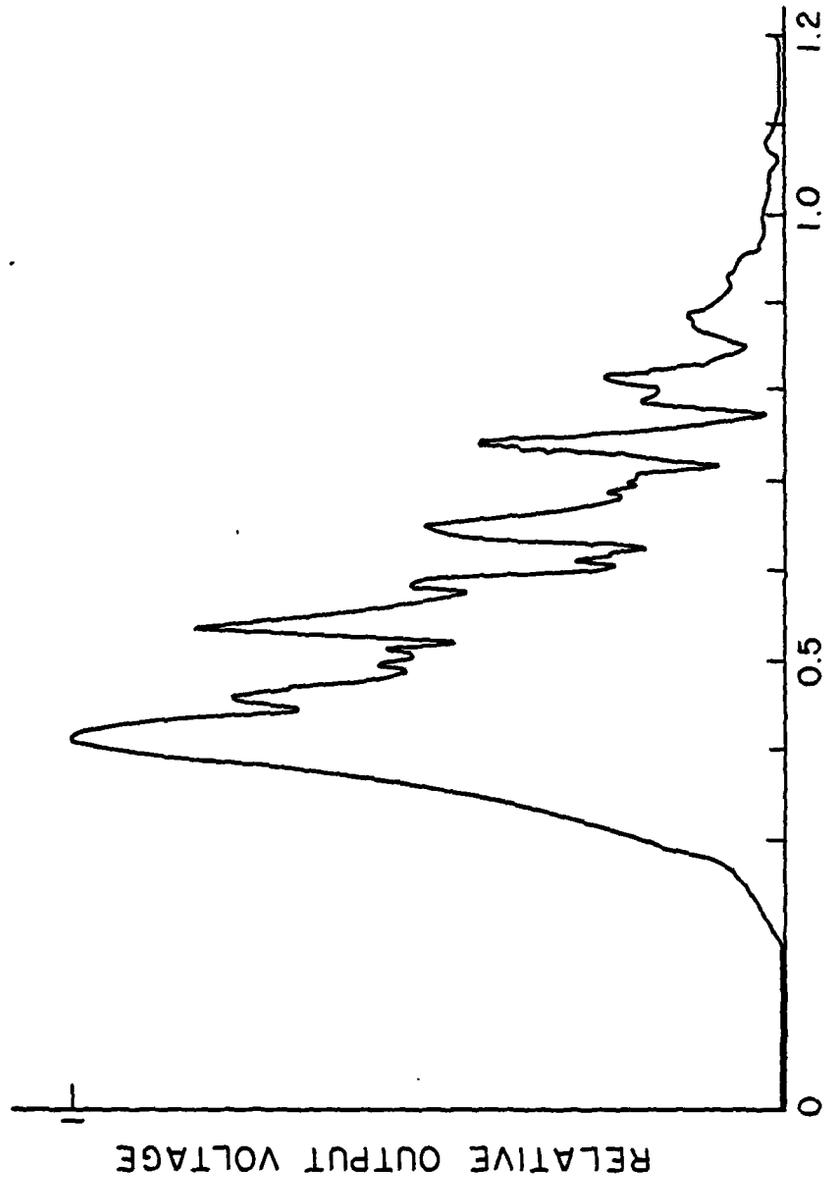

FIGURE 6. FREQUENCY RESPONSE OF ADMIRALTY SYSTEM AND TRANSDUCER – ACOUSTICALLY DRIVEN

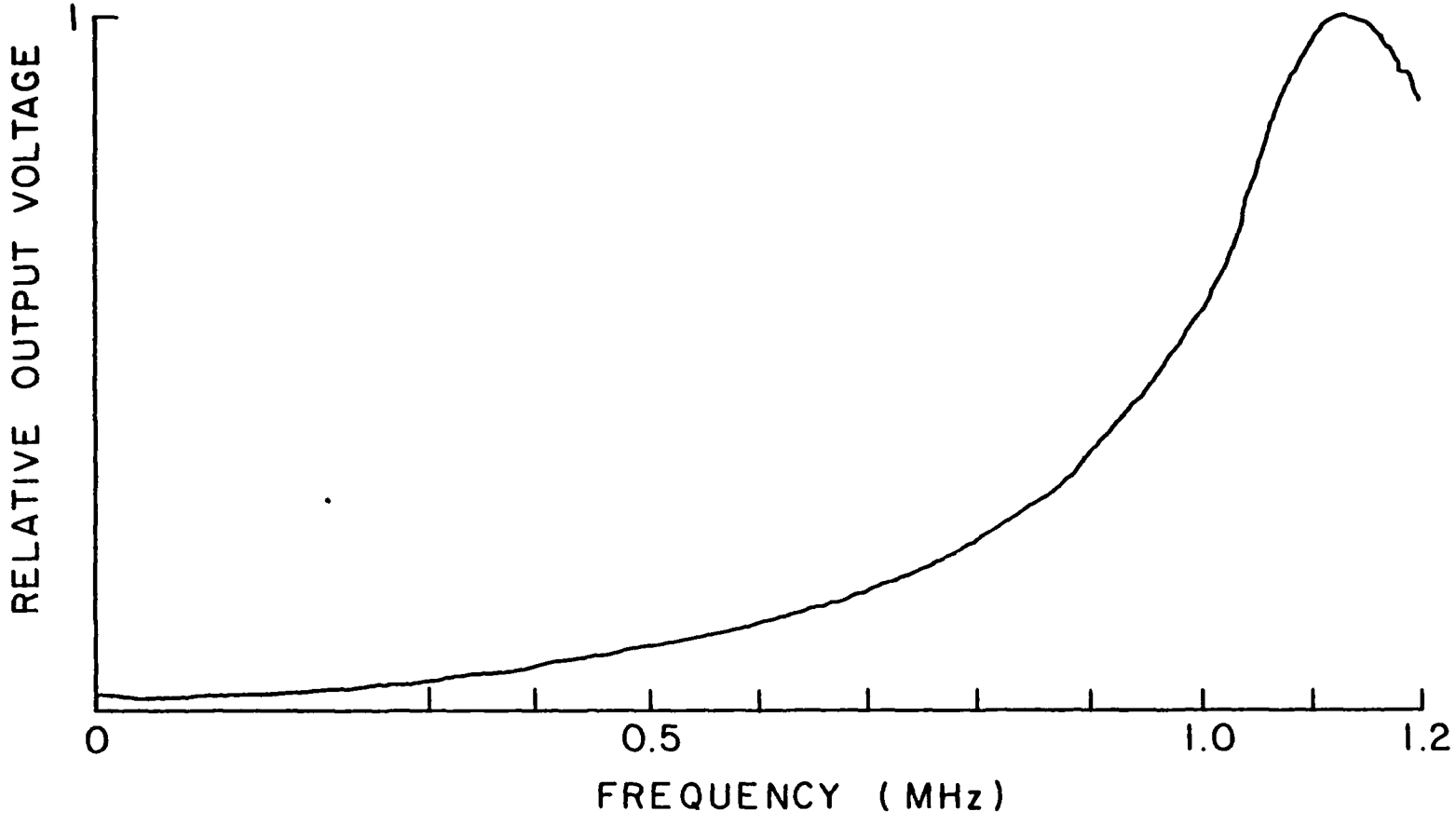

FIGURE 7. FREQUENCY RESPONSE OF AEROTECH TRANSDUCER ACOUSTICALLY DRIVING ADMIRALTY SYSTEM

to the preamplifier input. The system has provisions for time discrimination and event counting procedures for source localization, although these features were not needed in the present work. The electrical frequency response of the main amplifier, measured with none of the available band pass filters in use, is shown in Fig. 8. The frequency response of the system, again with no filtering, connected to a Panametrics Type AE-01-L transducer is shown in Fig. 9. The curve shown in Fig. 10, exhibiting the frequency response of the source transducer, demonstrates that the receiving transducer causes considerable coloration of the frequency response. The available band pass filters have excellent slope and rejection characteristics, as can be seen in Fig. 11, which is the frequency response curve of the system with the same Panametrics transducer and a 100 kHz-400 kHz filter. The rms noise floor measured 40 mV regardless of system gain indicating that the system performance was not limited by the preamplifier, but by later stages of amplification.

Eddy Current Examination

A Halec eddy current crack detector unit was used to search for the presence of surface cracks after the occurrence of a significant change in either ultrasonic attenuation or acoustic emission. This particular instrument operated at 3 MHz and was therefore only sensitive to surface breaking cracks. A pencil-shaped eddy current probe with a rounded tip permitted detection of surface cracks less than 1/16 in. long. A rounded tip was used rather than a flat one because of the greater relative ease with which contact with the

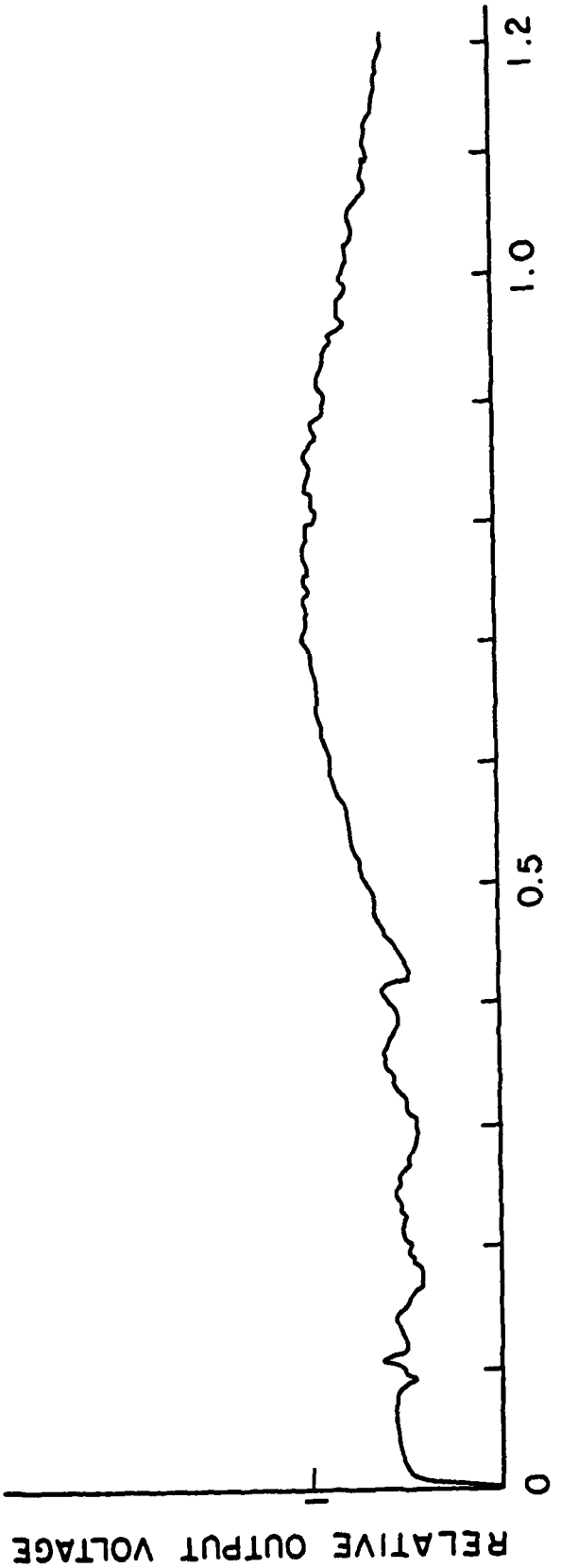

FIGURE 8. FREQUENCY RESPONSE OF TRODYNE AE SYSTEM AMPLIFIER

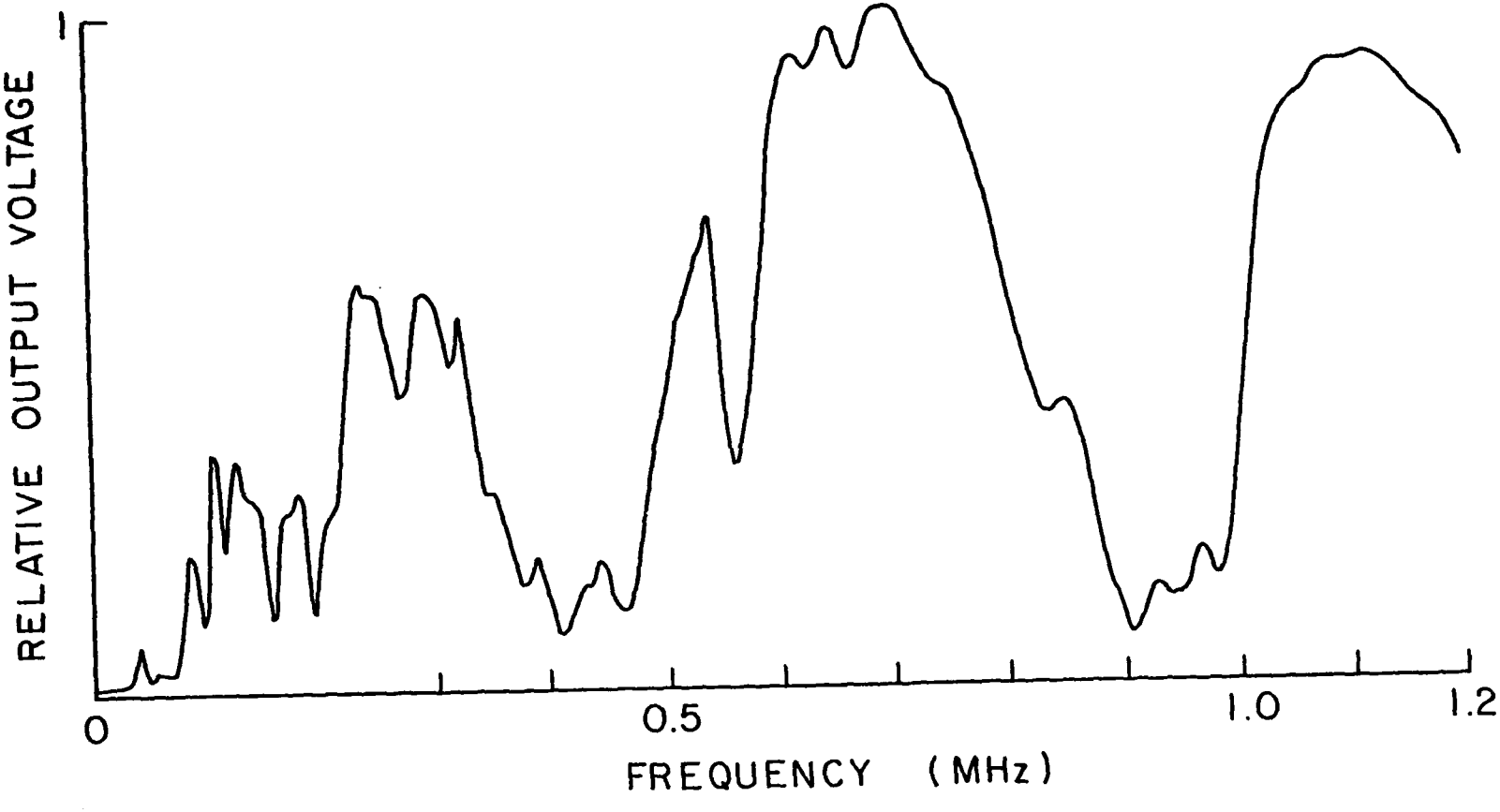

FIGURE 9. FREQUENCY RESPONSE OF TRODYNE SYSTEM AT FULL BANDWIDTH - ACOUSTICALLY DRIVEN

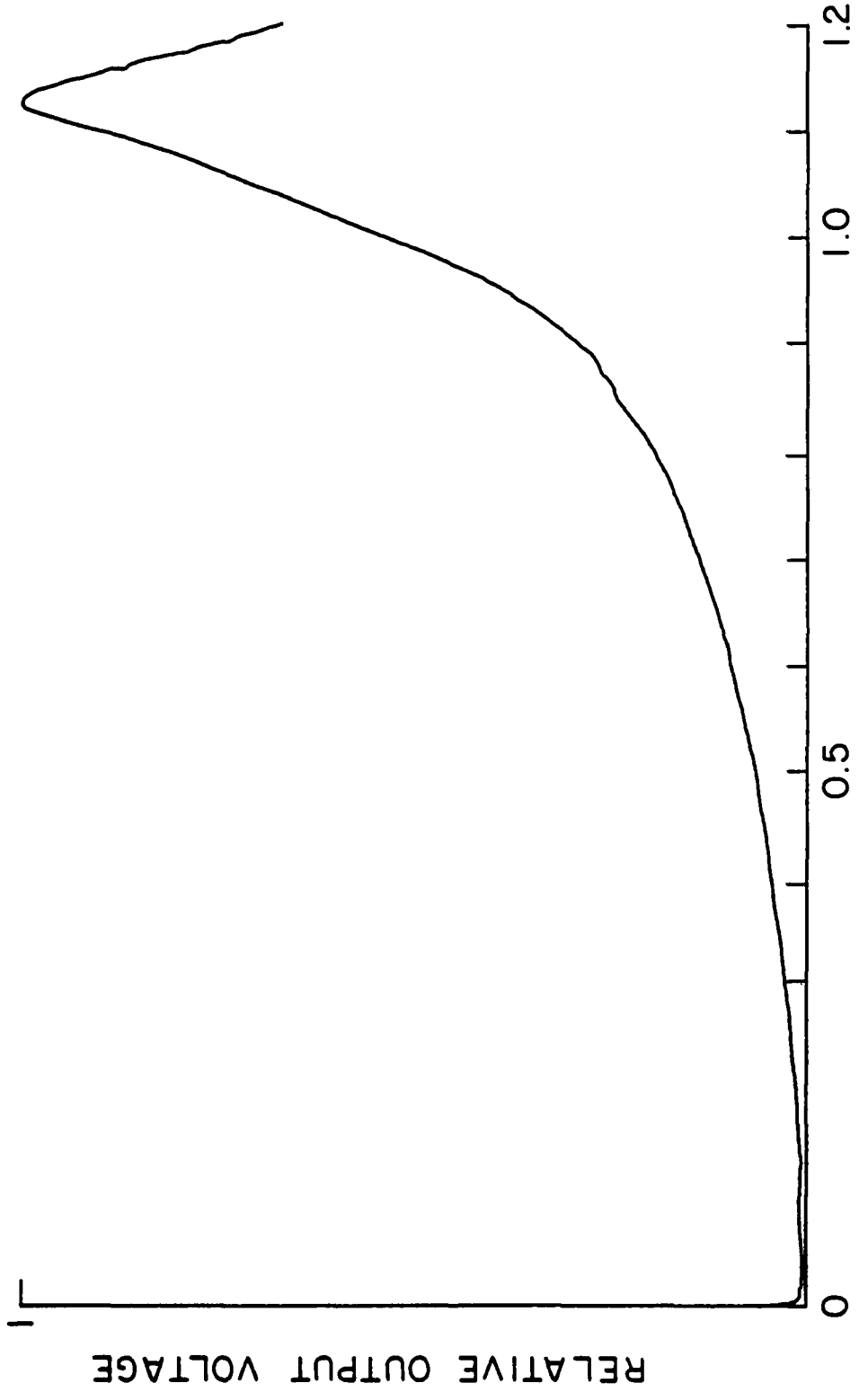

FIGURE 10. FREQUENCY RESPONSE AEROTECH TRANSDUCER ACOUSTICALLY DRIVING TRODYNE SYSTEM

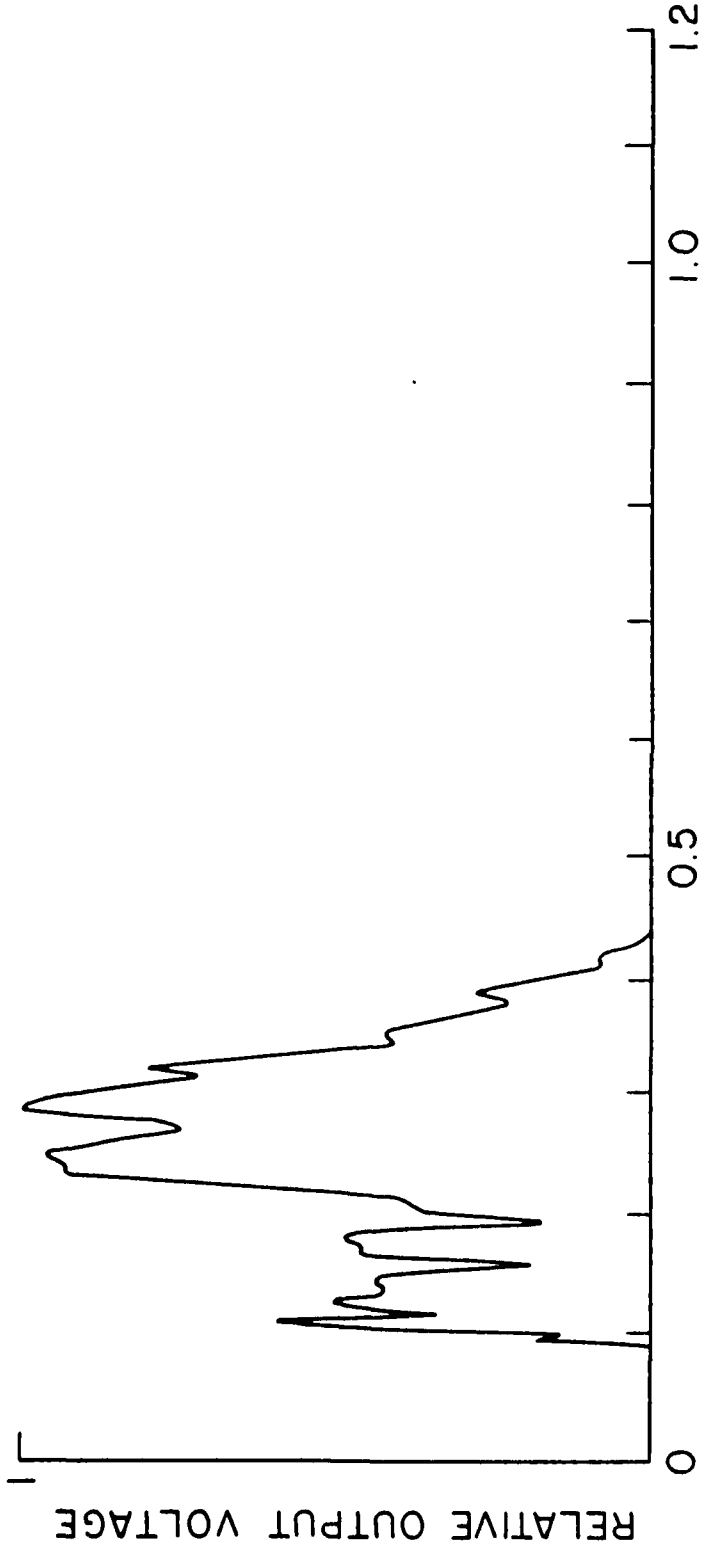

FIGURE 11. FREQUENCY RESPONSE OF TRODYNE SYSTEM
ACOUSTICALLY DRIVEN WITH 0.1-0.4 MHz
BANDPASS FILTER

specimen could be maintained. Another advantage of the rounded probe tip was its insensitivity to departures of as much as 15 deg. from the ideal positioning normal to the specimen surface. Although eddy current response is affected not only by specimen dimensions, geometry, and surface discontinuities, but also by the electrical conductivity and magnetic permeability of the specimen material, for 7075-T651 aluminum the changes in conductivity and permeability due to fatigue cycling are negligible. Since changes in the total area of metal surrounding the probe affect the signal, the probe was normally kept at least 1/8 in. from all specimen edges during scanning. Scans closer to the edges could be made by carefully adjusting the instrument. The utility of eddy current scanning of fatigue specimens is enhanced by the fact that the typical fatigue crack geometry is optimal for eddy current detection.

Metallographic Examination

After the presence of a crack was detected by a change in ultrasonic attenuation or acoustic emission and verified by eddy current probing, the fatigue test was either continued until the specimen fractured or the test was terminated and the specimen removed for metallographic examination. In the cases where the specimen fractured, the fracture surfaces were photographed in order to maintain a permanent record of the region of crack initiation and the region where the crack walls rubbed together after initiation. In the cases where the fatigue test was terminated prior to fracture, the region of the specimen surface close to the crack was carefully examined

with a Bausch and Lomb metallographic microscope capable of magnifications in excess of 5000X when an oil immersion objective was used. Subsequent to this surface examination, the specimen was sectioned and mounted in a metallographic mount. The mounted specimen was ground on successively finer grinding papers down to 600 grit and then polished on lapidary wheels using 15 μ and 0.05 μ compounds. In order to remove the cold-worked surface layer and to delineate the microstructure, the mechanically polished specimen was immersed in Keller's Reagent for 15 sec. and then plunged into 180° F water to remove the etchant. Finally the specimen was blown dry and clamped to the microscope stage. The specimen microstructure was examined for the presence of regions of high plastic deformation such as deformation bands, and for the effects of grain boundaries, inclusions, and precipitates.

Fatigue Test Results

To provide a data base and to verify expectations involving the effects of fatigue test amplitude, specimen geometry, and specimen surface preparation on fatigue life, a variety of tests was conducted. Table I contains details of tests run on sixteen specimens which possessed the geometry depicted in Fig. 1. Figure 12 shows a plot of bending stress versus number of fatigue cycles for the sixteen specimens listed in Table I as well as for four specimens (labeled A, B, C, D) which possessed sharp square-corners at the reduced cross-section shoulder. The use of a logarithmic scale to plot the number of fatigue cycles facilitated the compact display of the wide range of test durations. The different symbols in Fig. 12 represent the different

Specimen Number	Surface Condition	Vibration Amplitude (mm)	Bending Stress (Units of 10^4 psi)	Cycles to Crack Detection (Thousands)	Cycles to Fracture or Termination (Thousands)	Percent Fatigue Life to 0.5 dB Attenuation Change	Percent Fatigue Life to 1.0 dB Attenuation Change	Cycles Between Crack Initiation and Fracture (Thousands)
* 1	As-received	6.70	2.10	1383				
* 2	400 Grit	5.50	1.72	9119				
** 3	400 Grit	5.35	1.68		39800			
** 4	400 Grit	5.55	1.74		43000			
** 5	Rouge	5.50	1.72		25000			
6	Rouge	8.50	2.66		195	100	100	
7	Rouge	7.46	2.34	598	741	61	81	143
** 8	Rouge	6.48	2.03		12352			
9	Fine	6.91	2.17	10060	10100	99	100	40
10	Fine	6.91	2.17	6565	6673	98	99	108
11	Fine	6.98	2.19	9050	9050	100	100	
12	As-received	6.05	1.90	4140	4985	83	93	845
* 13	As-received	5.90	1.85	10724				
14	As-received	5.90	1.85	15624	16352	95	99	728
15	As-received	6.25	1.96	5694	5991	89	94	297
* 16	Rouge	6.98	2.19	5053				

TABLE I. DETAILS AND RESULTS

* Test terminated for metallographic examination

** Specimen removed from test after accumulation of at least 1.2×10^7 cycles with no sign of imminent failure

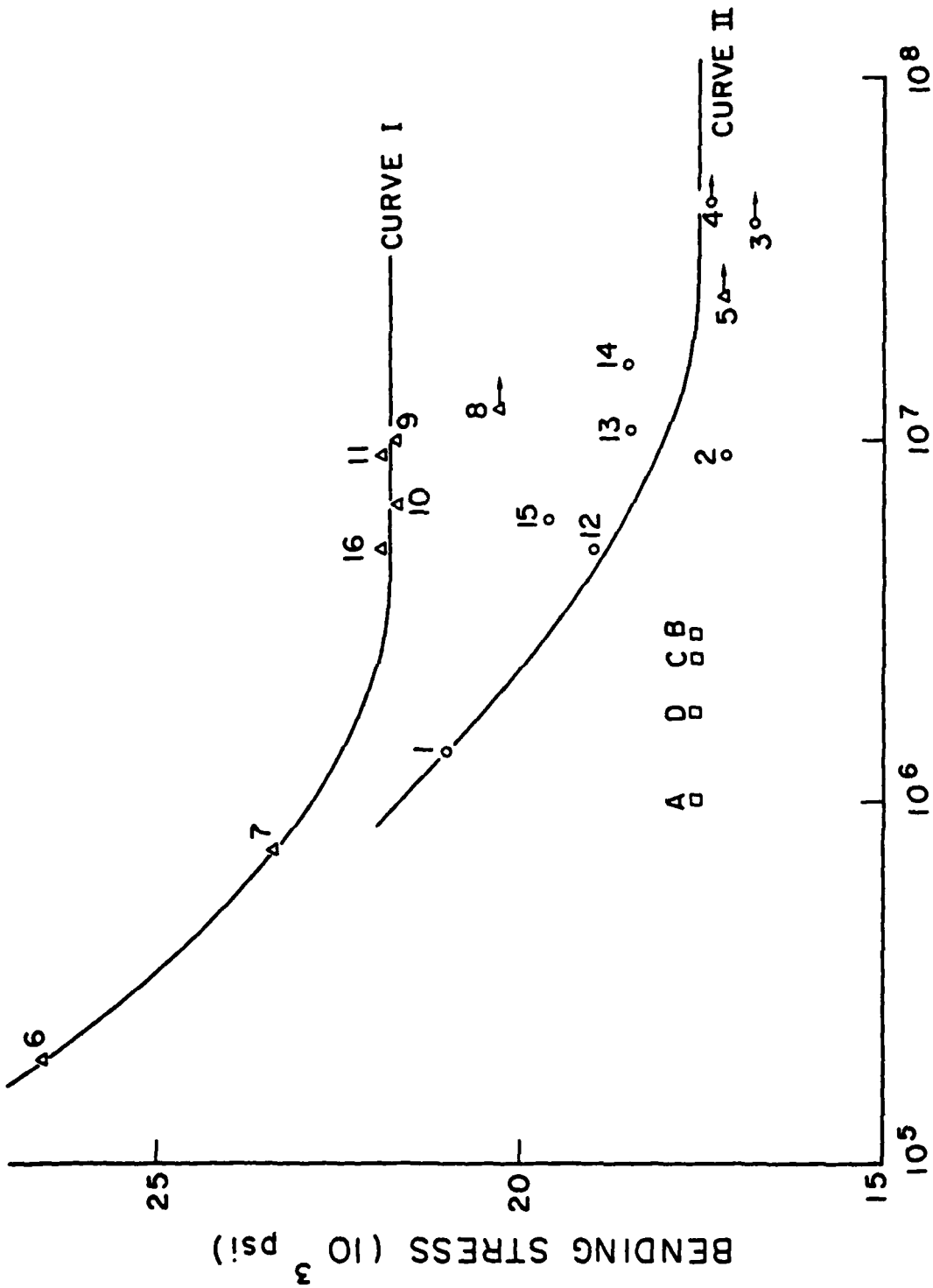

FIGURE 12. BENDING STRESS vs TEST DURATION

specimen surface preparations: triangles indicate fine or rouge polish, circles correspond to 400 grit polish, and squares denote the square-cornered shouldered specimens, all of which were tested in the as-received surface condition. Curve I of Fig. 12 is an approximate S-N curve for the rouge and fine polished specimens which were tested either until specimen fracture or until crack formation was detected and the fatigue test terminated. This curve exhibits the characteristic "knee" that defines a stress amplitude (endurance limit) below which the specimen can tolerate an indefinite number of fatigue cycles without fracturing. Since the fatigue testing arrangement used in the present research was somewhat different than that used to obtain American Society for Metals Handbook data, the endurance limit of 2.2×10^4 psi indicated in Fig. 12 may be considered to be in close agreement with the handbook value of 2.3×10^4 psi for 7075-T6 aluminum. The trend for specimens fatigued in the as-received surface condition or with 400 grit paper surface polish is not as clearly defined as that for the highly polished specimens. However, an approximate endurance limit can be estimated from Curve II. The arrows beside data point numbers 3, 4, 5 and 8 in Fig. 12 indicate that these specimens showed no sign of imminent failure after more than twelve million cycles.

Ultrasonic Attenuation Measurements

The initial ultrasonic attenuation and acoustic emission measurements conducted in the present research were made on specimens which possessed sharp square-corners at the reduced cross-section

shoulder. This design provided both a well defined pulse-echo pattern and a region where the fatigue damage should be localized in a manner compatible with eddy current scanning. However, it was found that the notch effect at the sharp corner caused a severe stress concentration causing premature crack formation and fracture. This problem was overcome by rounding the corners of the shoulder as shown previously in Fig. 1.

Early warning of fatigue failure attainable with ultrasonic attenuation was observed to be strongly dependent on specimen surface condition. Polishing the surface of the specimens necessitated an increase in the amplitude of bending (and hence the stress) required to initiate failure in a given number of cycles. This increase in fatigue life due to surface polishing can be explained by considering any surface irregularity as a potential crack initiation site. Polishing reduces the number and severity of surface irregularities and thus greatly decreases the number of potential crack initiation sites.

As mentioned earlier, the ultrasonic attenuation measurements made during the present research were not conventional attenuation measurements in that the attenuation values recorded were not obtained from the amplitude ratio of two successive reflections from the same part of the test specimen. Instead the amplitude of the first reflection from the specimen shoulder was compared with the amplitude of the first reflection from the specimen end. This was done for two reasons. First, these two reflections had larger amplitudes than any of the other detectable reflections, and second,

it was thought that this procedure would enhance system sensitivity to crack formation. Since crack initiation occurs near or in the plane of the shoulder, and since there is reflection of ultrasound from the crack, the first reflection from the shoulder is increased by crack formation. On the other hand, a crack at the shoulder will disperse ultrasound traveling the full length of the specimen and thus reduce the amplitude of the first reflection from the specimen end. Hence, the relative change of the ratio of the amplitudes of the reflections from the shoulder and specimen end will be greater than that of two successive reflections from the specimen end.

In nine out of ten tests on specimens fatigued until crack formation occurred, the presence of a crack easily detectable by eddy current scanning was indicated by at least an 0.5 dB change in ultrasonic attenuation. Included in Table I are the percentages of elapsed fatigue life where 0.5 and 1.0 dB changes in ultrasonic attenuation were recorded. In two cases the 0.5 dB change in attenuation observed was a decrease rather than an increase. All 1.0 dB attenuation changes were increases and portended imminent failure. In the last column of Table I, the number of fatigue cycles between crack detection and specimen fracture is indicated.

Figures 13 and 14 show typical change in ultrasonic attenuation versus percent fatigue life curves for highly polished and as-received surface condition specimens fatigued to fracture. Ultrasonic attenuation gave earlier warning of fatigue damage for specimens in the as-received and slightly polished surface condition than for

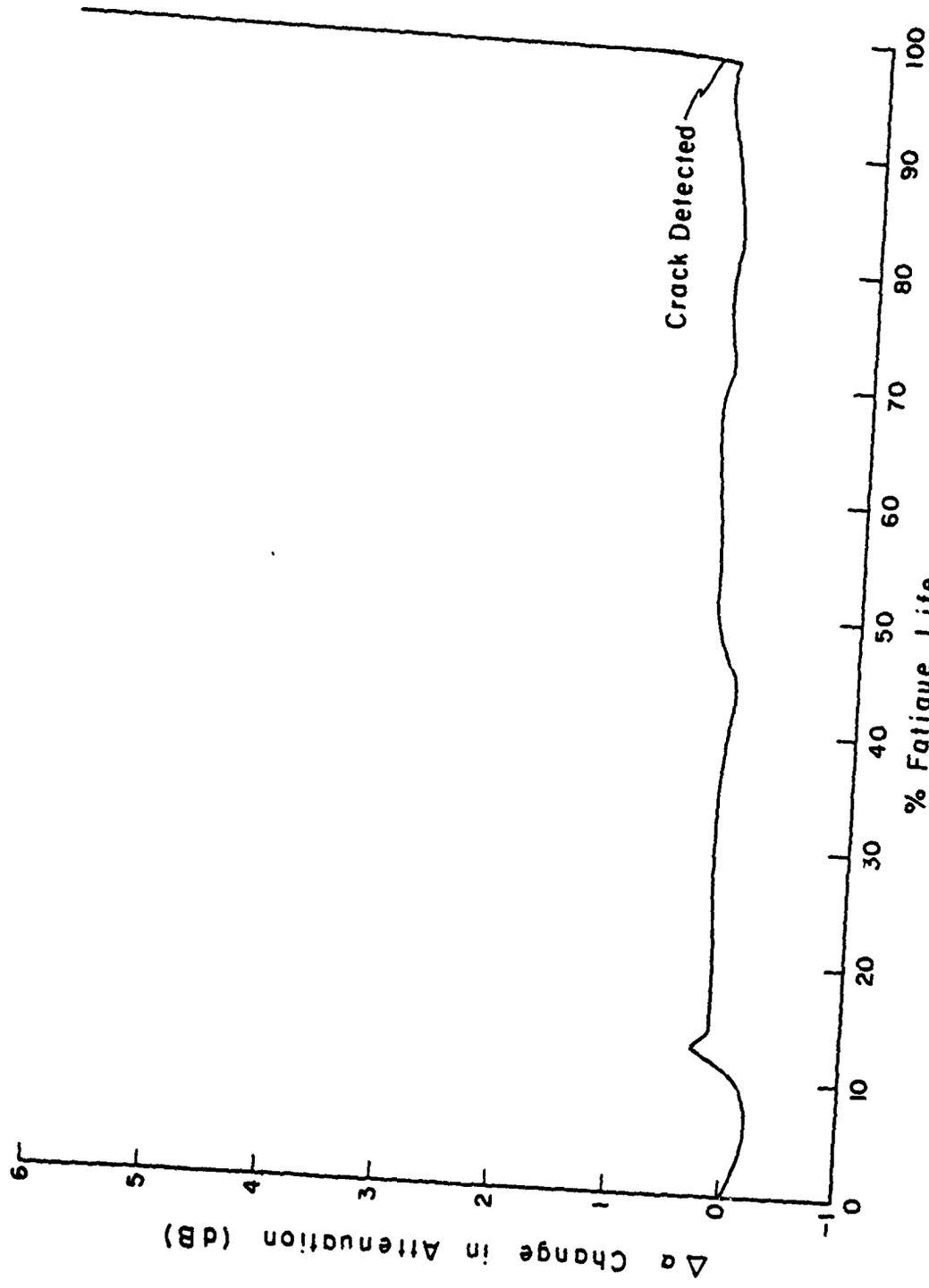

FIGURE 13. ULTRASONIC ATTENUATION vs FATIGUE LIFE FOR A TYPICAL HIGHLY POLISHED FATIGUE SPECIMEN

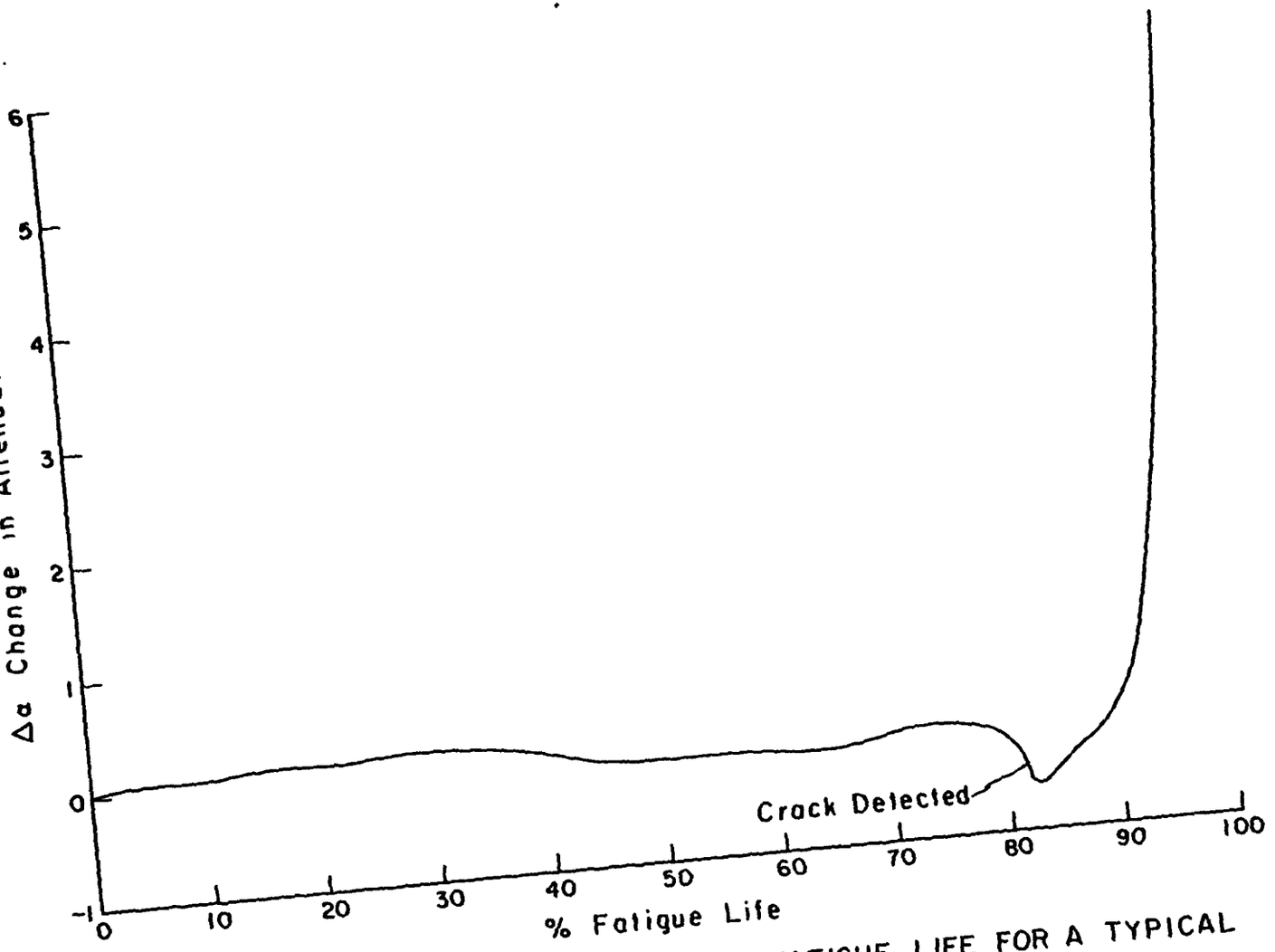

FIGURE 14. ULTRASONIC ATTENUATION vs FATIGUE LIFE FOR A TYPICAL AS-RECEIVED FATIGUE SPECIMEN

specimens with highly polished surfaces. Comparison of the experimental results obtained for specimens 10 and 15 show that, for fatigue tests of similar length, the number of fatigue cycles from crack initiation to specimen fracture was 2.97×10^5 for the as-received specimen (15) and only 1.08×10^5 for the highly polished specimen (10). In both cases, when surface crack initiation occurred, the ultrasonic attenuation changed significantly. Several explanations for this observed behavior are possible. Consider the well-established fact that polishing increases the fatigue strength, i.e., the stress at which, for a given number of cycles, a specimen will fail. Thus, for the tests of comparable length run during the present research, the more highly polished specimens were fatigued at higher stress amplitudes than the as-received and less polished specimens. In spite of the higher stress amplitudes, crack initiation occurred later in the fatigue life of the polished specimens. This delay in crack initiation can be attributed to the reduction in number and severity of potential crack initiation sites as a result of surface polishing. Since crack initiation is invariably accompanied by substantial changes in ultrasonic attenuation, this explanation is consistent with the experimental results. The relative lack of early warning obtained with the highly polished specimens is also consistent with two other factors. First, a highly polished specimen will fracture faster, once a crack has been initiated, because of the higher stress amplitude being applied during the fatigue test. Second, because of the higher stress amplitude

and longer test duration prior to crack initiation, the highly polished specimens will have sustained more extensive bulk damage than the less polished specimens. Once initiated, the crack propagates easily and rapidly through the highly polished specimen until fracture. This severely limits the amount of early warning attainable by ultrasonic attenuation monitoring. In the case of the as-received and less polished specimens, earlier warning was possible because at the time of crack initiation the surrounding material was still relatively unchanged except for a small plastically deformed region around the crack tip and sides.

A pulse-echo pattern as photographed from the monitoring oscilloscope after a test specimen had exhibited crack initiation is shown in Fig. 15. Comparison of this pattern with the pattern photographed prior to fatigue crack initiation, Fig. 4, reveals several significant differences. The amplitude of the first reflection from the specimen end, peak C, is much smaller in Fig. 15 than in Fig. 4. This decrease in amplitude of peak C is caused both by the enhanced reflection from and diminished transmission through the crack, and by the action of the automatic gain control circuitry in the attenuation recorder. Any increase in the amplitude of the first reflection from the shoulder, peak A, is cancelled by the automatic gain control, which by decreasing the overall system gain effectively decreases the amplitudes of all other echoes.

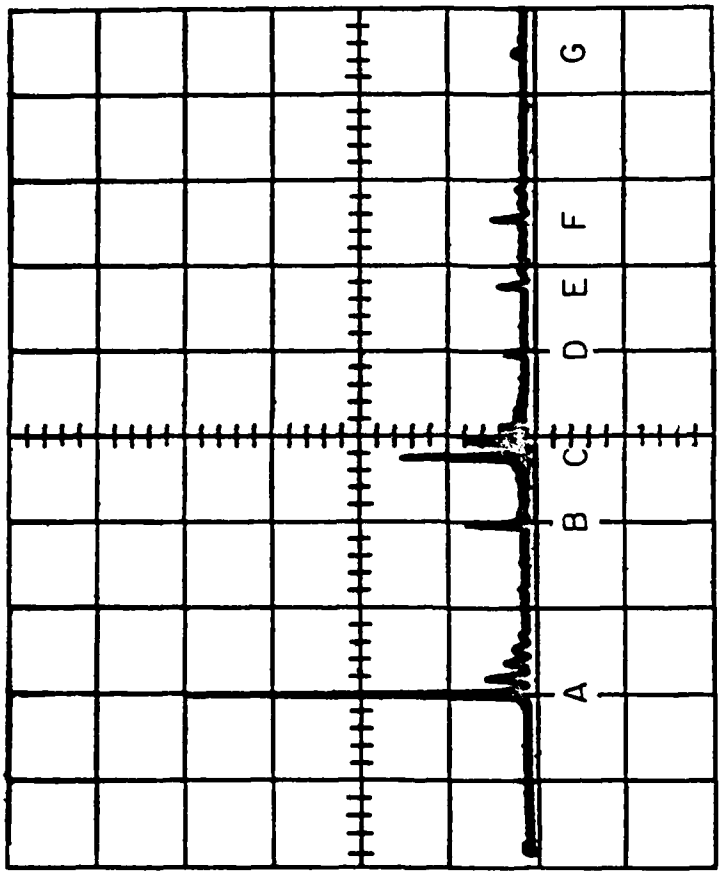

FIGURE 15. TYPICAL PULSE-ECHO PATTERN AFTER CRACK INITIATION WITH SIGNIFICANT PEAKS LETTERED

Crack detection can also be accomplished by inspection of the pulse-echo waveform. Although the use of a reduction in cross-section to localize crack formation causes a large reflection of ultrasound from the shoulder thus created, the appearance of new echoes signalling crack initiation is not precluded. For example, peak F in Fig. 15 has no counterpart in Fig. 4. The time of arrival for echo F corresponds to a reflection from the specimen end, followed by a reflection from the crack, a second reflection from end, and finally transmission of the pulse past the crack to the transducer. It follows from the specimen geometry that the decrease in cross-sectional area at the shoulder causes partial reflection of a pulse traveling away from the transducer, but has an insignificant effect on a pulse traveling from the specimen end to the transducer. Echoes B and D in Fig. 15, the second and third reflections from the shoulder-crack plane, show increased amplitudes relative to their counterparts in Fig. 4. This illustrates the increased reflectivity caused by the presence of the crack. The reflection-transmission explanation presented earlier is also supported by the decrease in amplitude of echo G in Fig. 15 compared with Fig. 4. This echo, which is due to the second reflection from the specimen end, has traversed the shoulder plane four times and is therefore greatly attenuated when a crack is present.

Acoustic Emission Measurements

Acoustic emission data was gathered using the two systems described earlier. In the absence of any a priori information

suggesting a different approach, the frequency responses of the two systems were selected to be approximately equal. As expected, the observed differences in system performance and in the data itself from the two systems were negligible.

In contrast to the situation with ultrasonic attenuation monitoring, considerable acoustic emission activity in the form of burst emissions transpired early in the fatigue tests. A typical set of burst waveforms, one from each system, is shown in Figs. 16 and 17. The relatively long, 1.5 msec, duration of the bursts is probably due to multiple reverberations inside the specimens. The frequency spectra corresponding to the waveforms reproduced in Figs. 16 and 17 appear in Fig. 18. The presence of many sharp peaks in both spectra, rather than a smooth more continuous curve, supports the hypothesis that high order vibrational modes were present. In the spectrum obtained using the Admiralty system, the peak at 98.6 kHz corresponds to the frequency calculated by assuming vibrational nodes at the specimen end and at the plane through the shoulder. The presence of many adjacent peaks is not surprising, considering the complicated specimen shape. Anticipated refinements in procedure and equipment are expected to enable improved burst waveform characterization in both time and frequency domains.

The general trend provided by continuous monitoring of acoustic emission also provided insight into the general nature of fatigue damage. In Fig. 19 the relative changes in the averaged root-mean-square voltage output of both the Admiralty and Trodyne

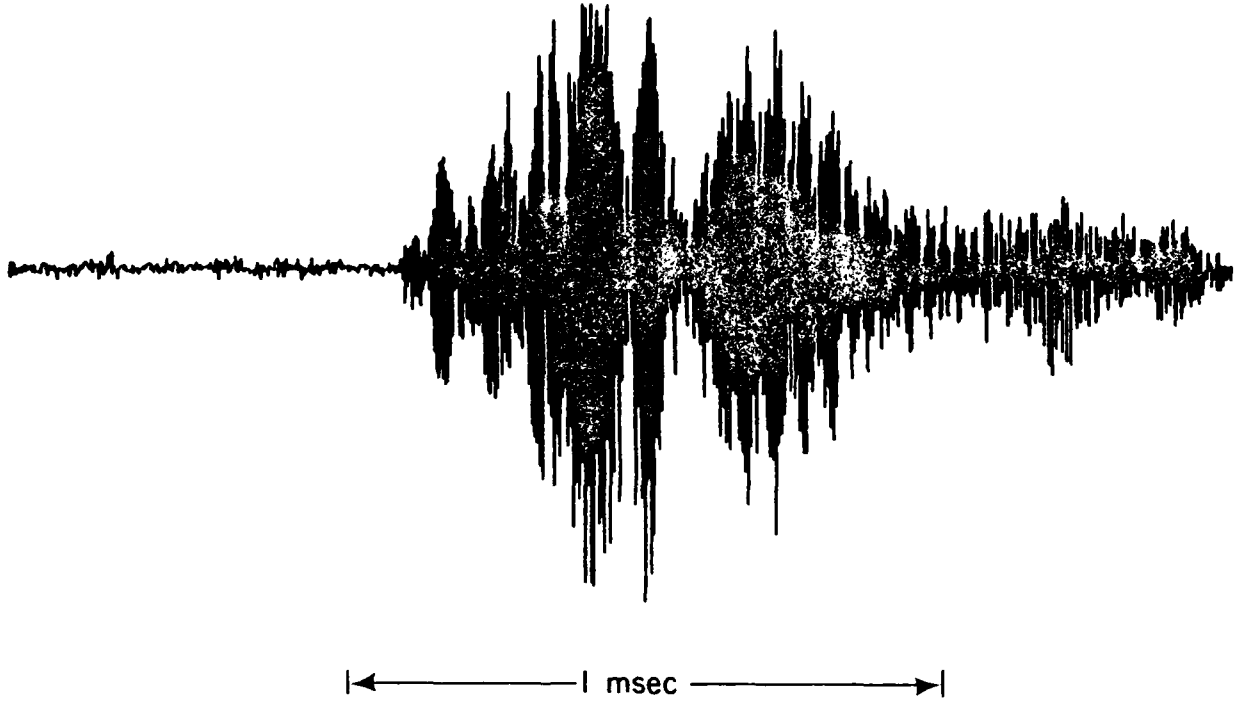

FIGURE 16. TYPICAL ACOUSTIC EMISSION BURST WAVEFORM — ADMIRALTY SYSTEM

tions. The different symbols in Fig. 12 represent the different

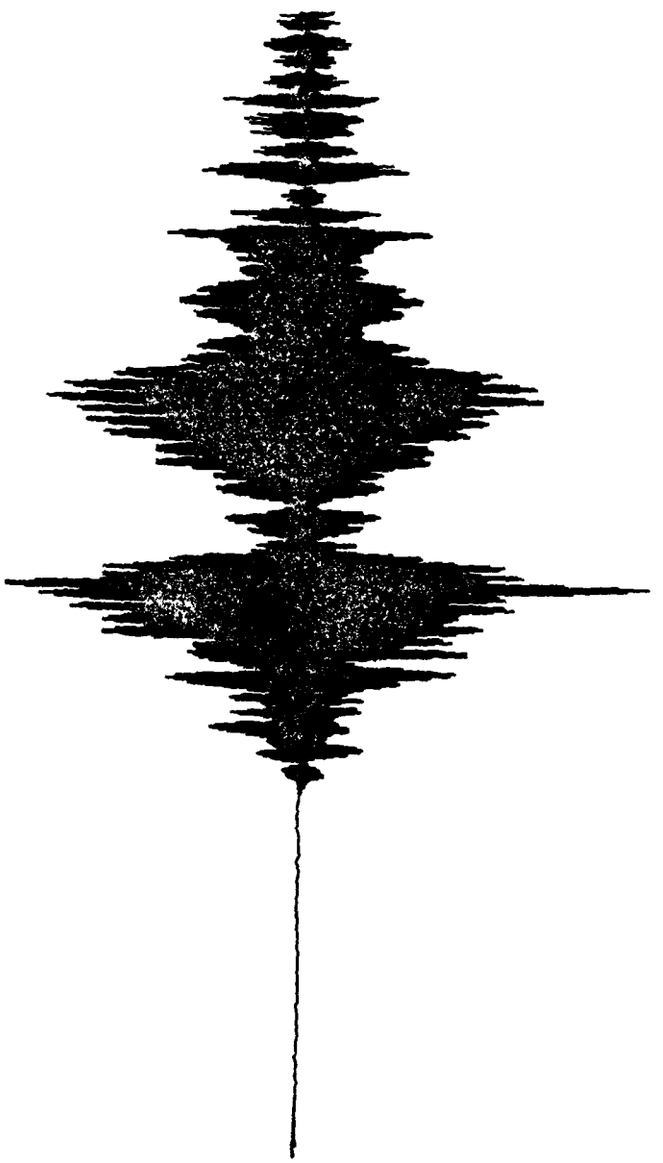

FIGURE 17. TYPICAL ACOUSTIC EMISSION BURST WAVEFORM – TRODYNE SYSTEM

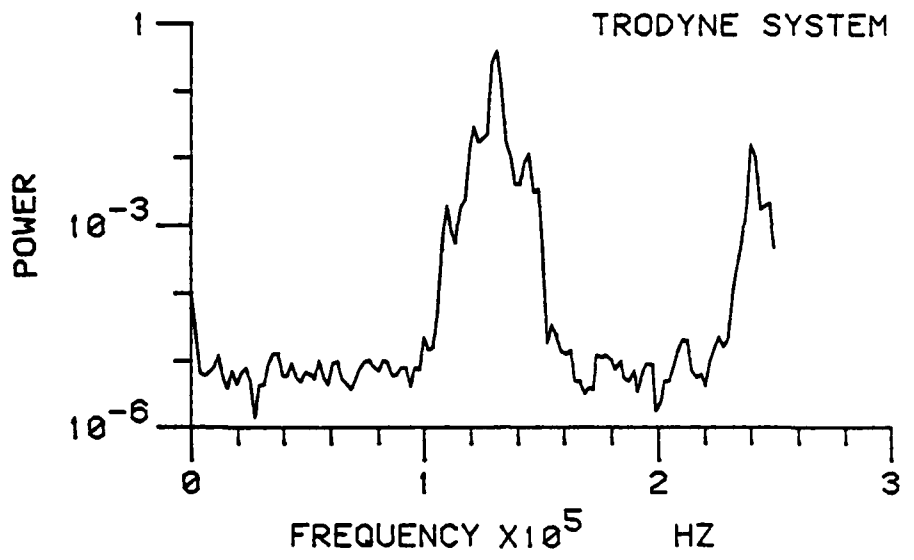

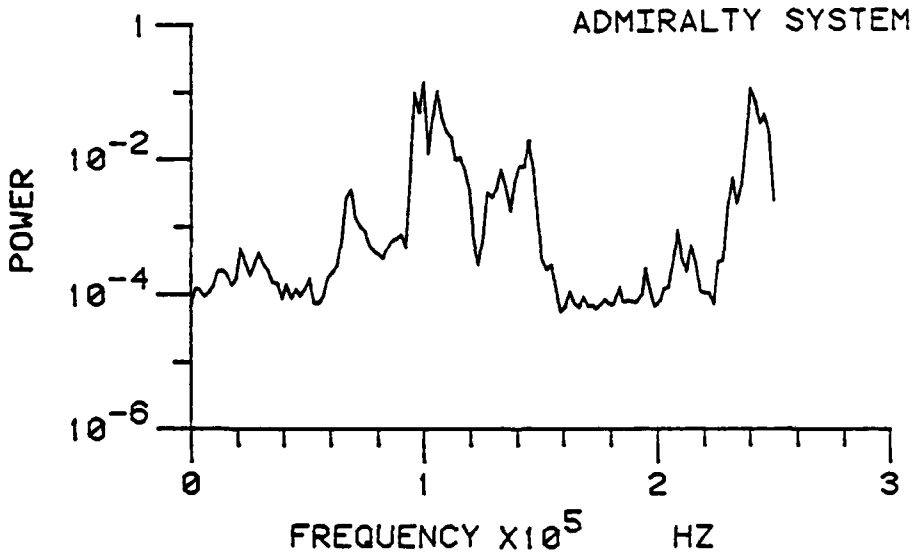

FIGURE 18. FREQUENCY SPECTRA OF TYPICAL ACOUSTIC EMISSION BURST WAVEFORMS

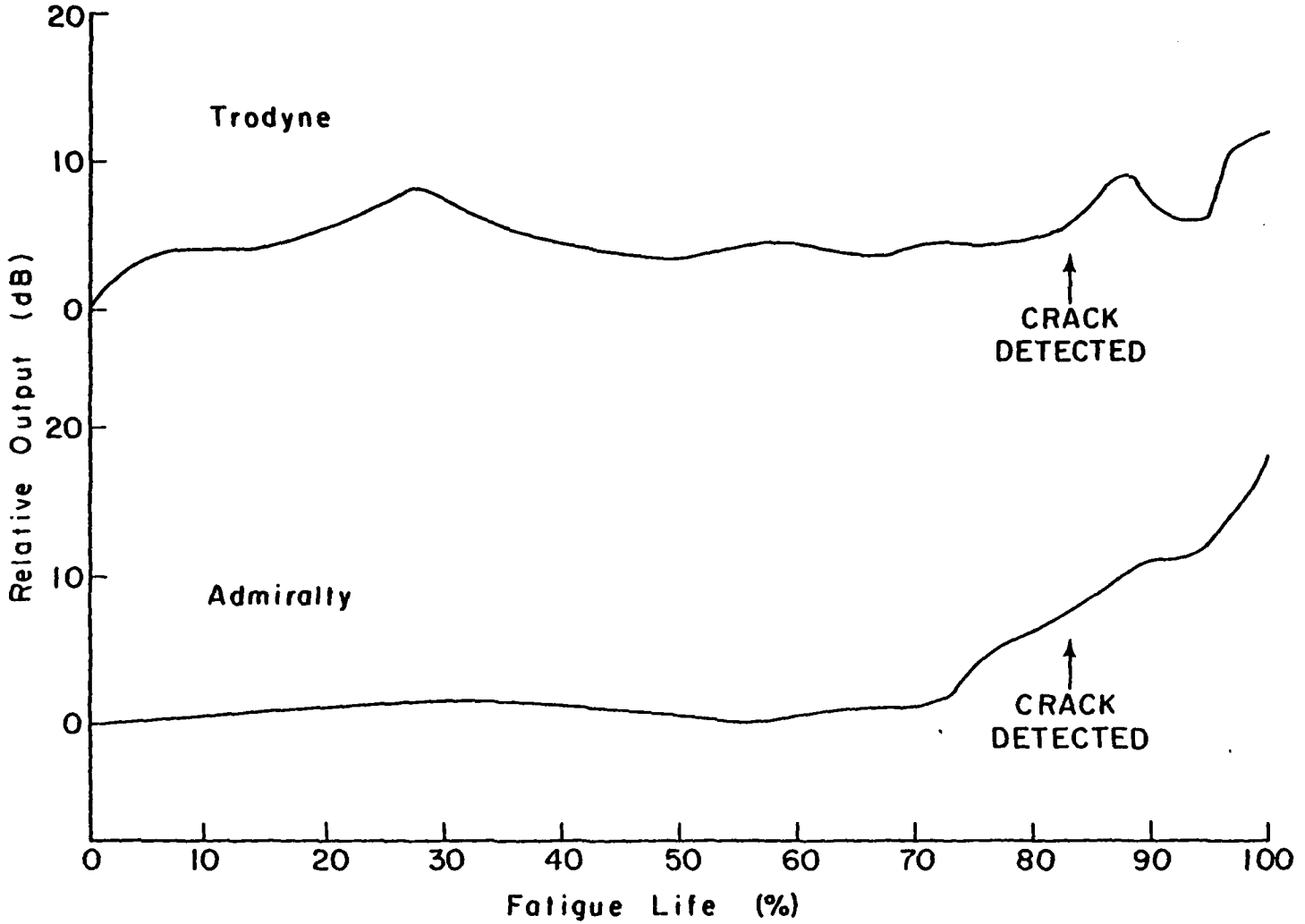

FIGURE 19. TYPICAL ACOUSTIC EMISSION RECORD (Averaged RMS)

systems are displayed. As shown, the overall acoustic emission level increased when a crack formed and propagated. This was probably caused by the newly created crack walls abrading against each other during subsequent fatigue cycles. Selected portions of an actual rms acoustic emission record as recorded on the strip-chart recorder are shown in Fig. 20. It should be noted that, in addition to a general increase in the overall acoustic emission level following crack initiation, the intensity of the bursts decreased as the specimen approached fracture. The relatively long time constant of the instrumentation used thus far precluded detailed interpretation of the spikes in the strip-chart record. Experimentation with improved instrumentation is currently being conducted in order to identify the origin and nature of this behavior.

Eddy Current Examination

After the set-point circuit stopped the fatigue machine when an 0.5 dB change in ultrasonic attenuation occurred, eddy current scanning was used to verify the presence of a surface crack. Due t the symmetric loading, there were four highly probable sites for crack initiation on each specimen. These sites were located at the four corners of the reduced cross-section shoulder. The presence of multiple potential crack initiation sites precluded any simple continuous eddy current monitoring. Conceivably, a complex mechanical scanning device could be designed and constructed if continuous eddy current scanning was deemed necessary.

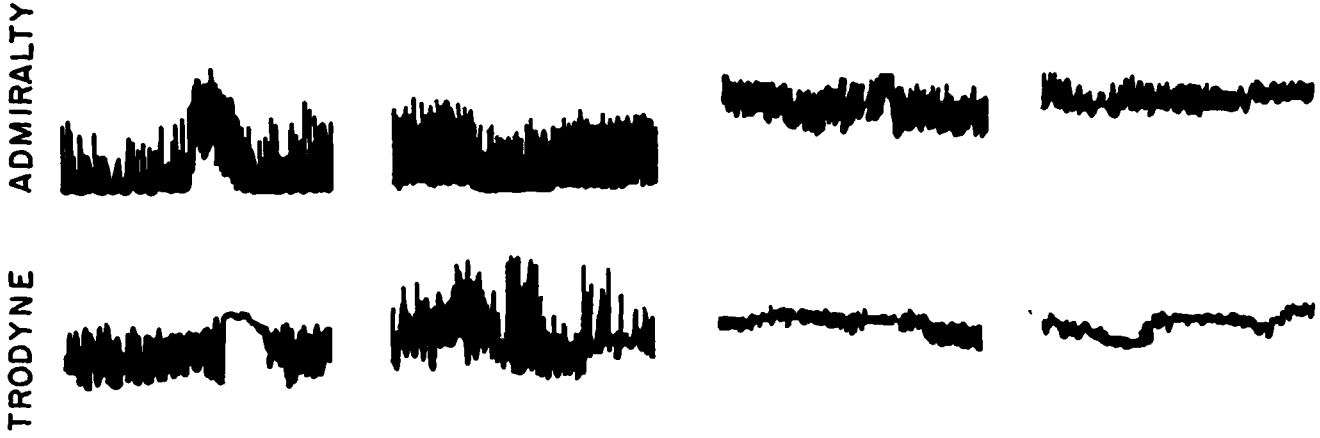

FIGURE 20. SELECTED PORTIONS OF AN ACOUSTIC EMISSION RECORD FOR A TYPICAL SPECIMEN

After the presence of a crack was confirmed, further eddy current scanning was employed in order to determine the length and relative severity of the crack. Such a series of scans for a typical fatigue specimen is shown in Fig. 21. The eddy current pencil probe was used to scan along the specimen length at 0.01 in. intervals starting 0.1 in. from the specimen edge. The amplitudes of the peaks represent the relative severity (depth) at different locations along the crack. The positions of the peaks represent the position of the crack along the scanned specimen length. The scans shown in Fig. 21 indicate that the crack scanned was perpendicular to the specimen length and originated at the top edge of the scanned width. This scanning procedure gave a very accurate and fast method of crack location and size. When it was decided to continue the fatigue test to specimen fracture, the propagation of the crack across the specimen surface could be easily monitored using eddy current scanning. This was of particular importance when testing specimens with as-received surfaces, because the crack was undetectable usually in its early stages.

Metallographic Examination

Metallographic analysis performed on the fatigued specimens showed several interesting features. Figure 22 indicates schematically the location of a typical crack on the specimen surface. For all specimens tested, the crack initiated on the surface at one of the four corner sites previously mentioned. Figure 23 indicates the location on the specimen of the fracture surfaces displayed in the typical

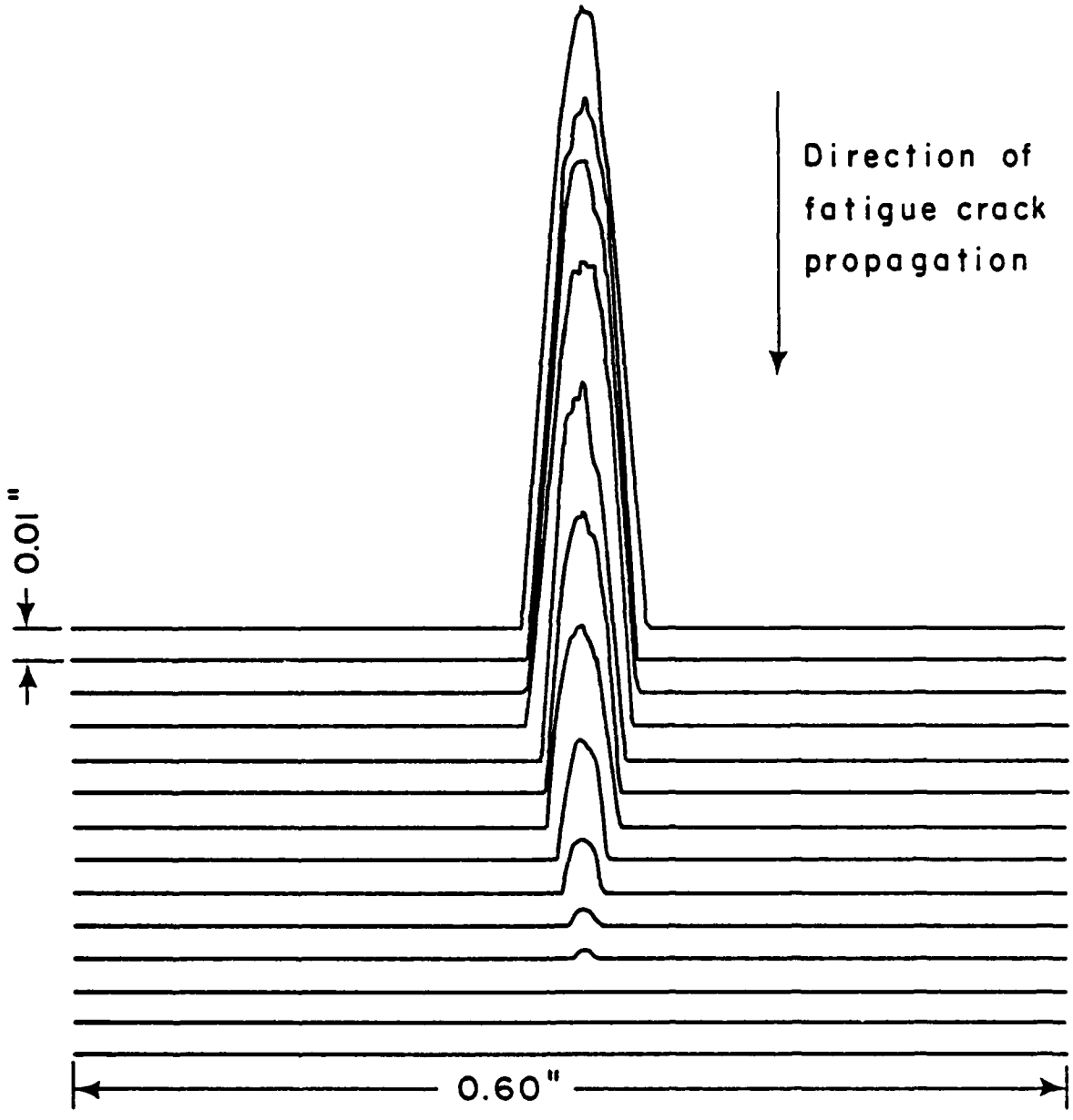

FIGURE 21. SERIES OF EDDY CURRENT SCANS OF A SURFACE FATIGUE CRACK. AMPLITUDE REPRESENTS RELATIVE CRACK SEVERITY. SCANS ARE 0.01 IN. APART STARTING 0.10 IN FROM SPECIMEN EDGE.

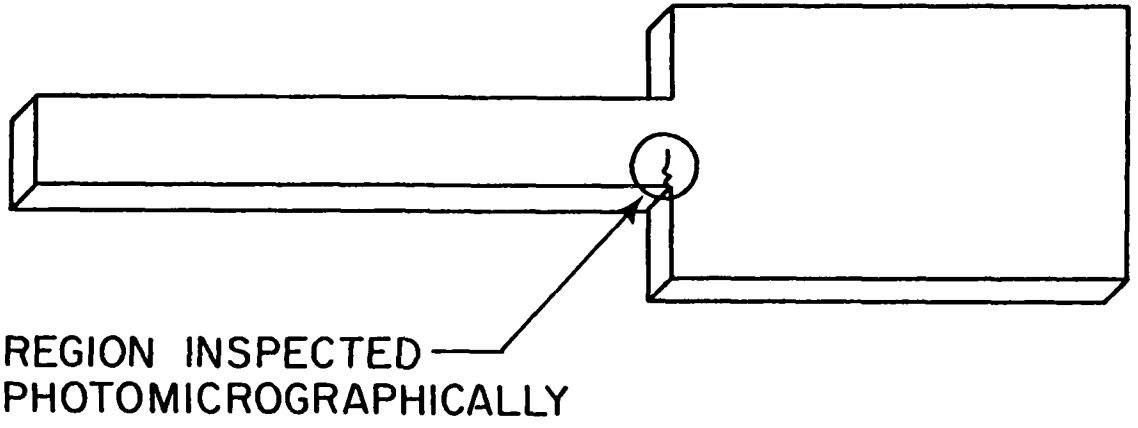

FIGURE 22. SCHEMATIC REPRESENTATION OF FATIGUE CRACK REGION

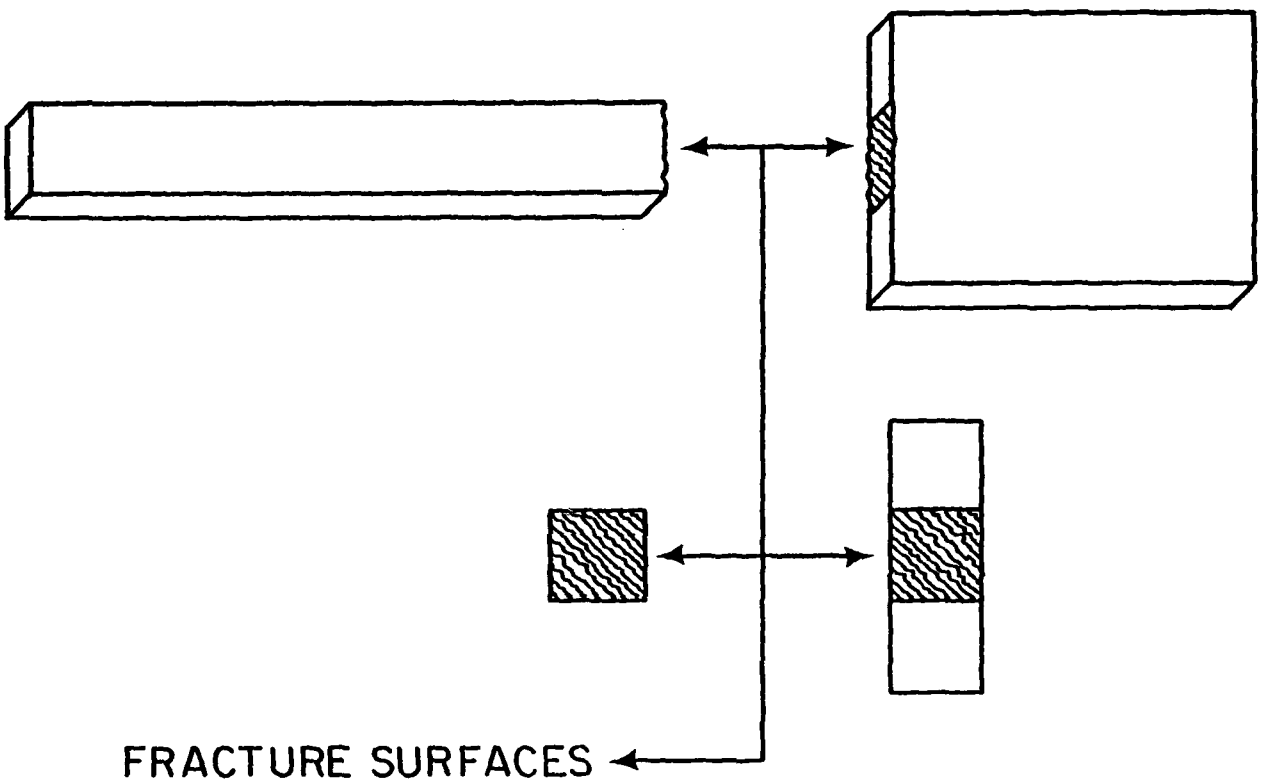

FIGURE 23. SCHEMATIC REPRESENTATION OF FRACTURE SURFACES (FRACTOGRAPHS)

fractographs of Figs. 24, 25, 26 and 27. Figures 24 and 25 show the fracture faces of specimen 14, which was fatigued in the as-received condition to complete fracture at a stress amplitude of 1.85×10^4 psi. For this specimen the crack originated at the lower left corner of the specimen as viewed in the fractograph shown in Fig. 24. The corresponding location in Fig. 25 is the upper left corner. Both of these figures show darkened regions and a very irregular surface near the corner where the crack initiated. Rubbing of the crack faces during cyclic bending accounts for the very dark areas, while the general irregularity of the surface is due to the brittle nature of the early phase of fatigue cracking. As the crack progressed through the bulk of the specimen, the effective cross-section subjected to the cyclic forces of reverse bending was reduced. Thus, for a constant vibration amplitude, the effective stress was increased, causing the crack to propagate at an increasing rate.

Comparison of Figs. 26 and 27 with Figs. 24 and 25 reveals the difference between the fracture surfaces obtained from specimens having a fine surface polish and those possessing an as-received surface. Figures 26 and 27 are fractographs from specimen 7, which possessed a polished surface. The light areas of Figs. 26 and 27 are significantly larger than those of Figs. 24 and 25, indicating a greater amount of work hardening in the material due to the higher stress applied over a greater number of cycles, prior to crack initiation in the polished specimens. Conversely, the rougher

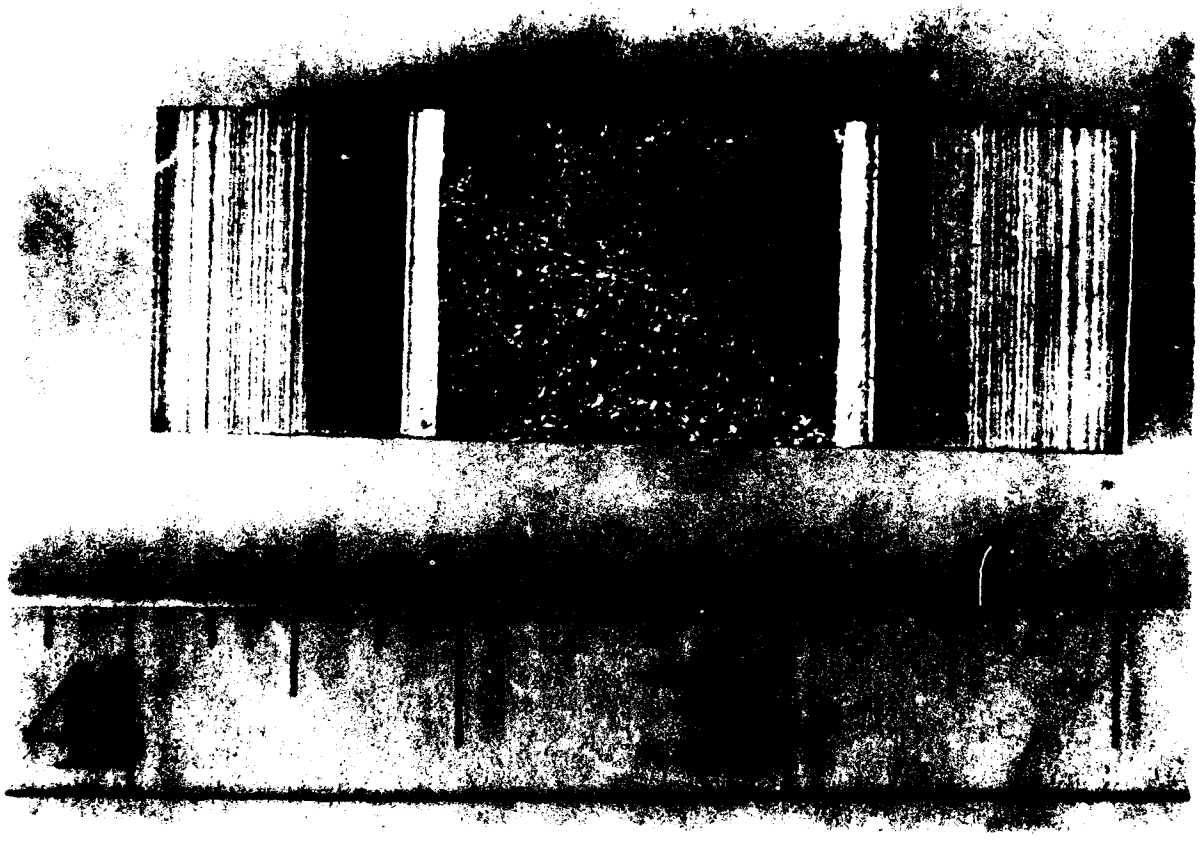

FIGURE 24. FRACTOGRAPH OF SPECIMEN 14 (FIXED PORTION)

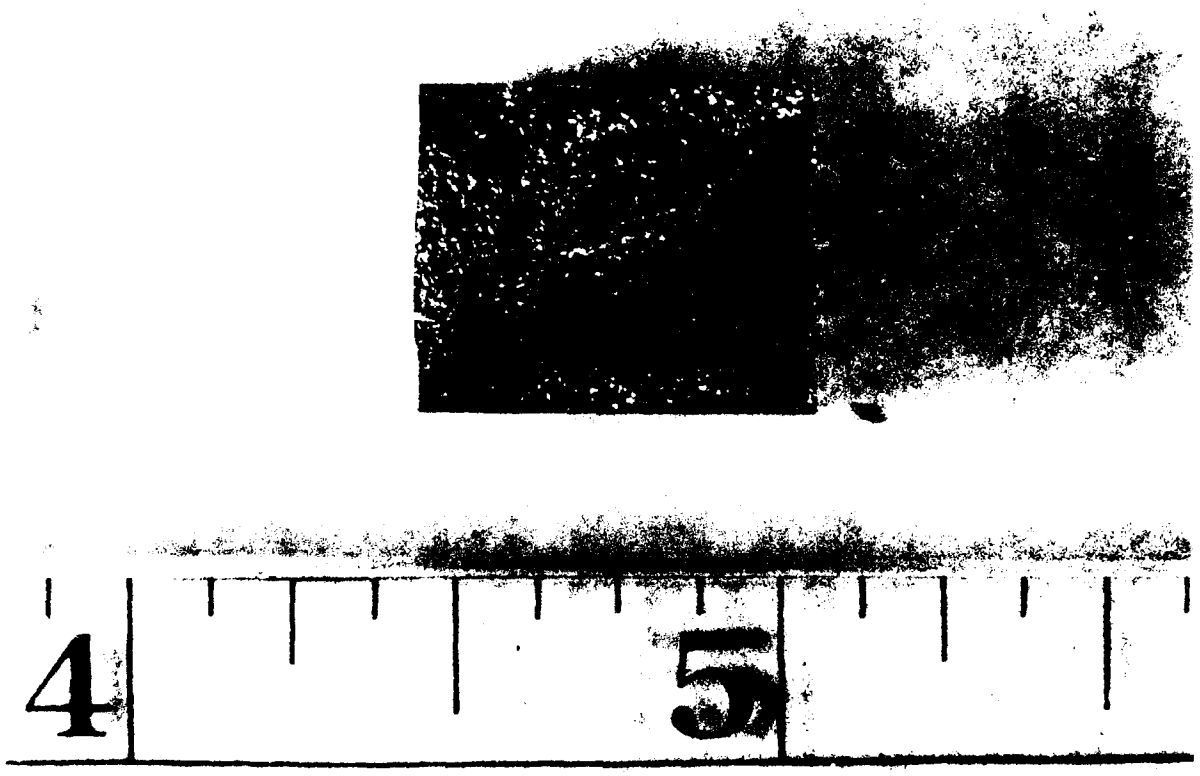

FIGURE 25. FRACTOGRAPH OF SPECIMEN 14 (DRIVEN PORTION)

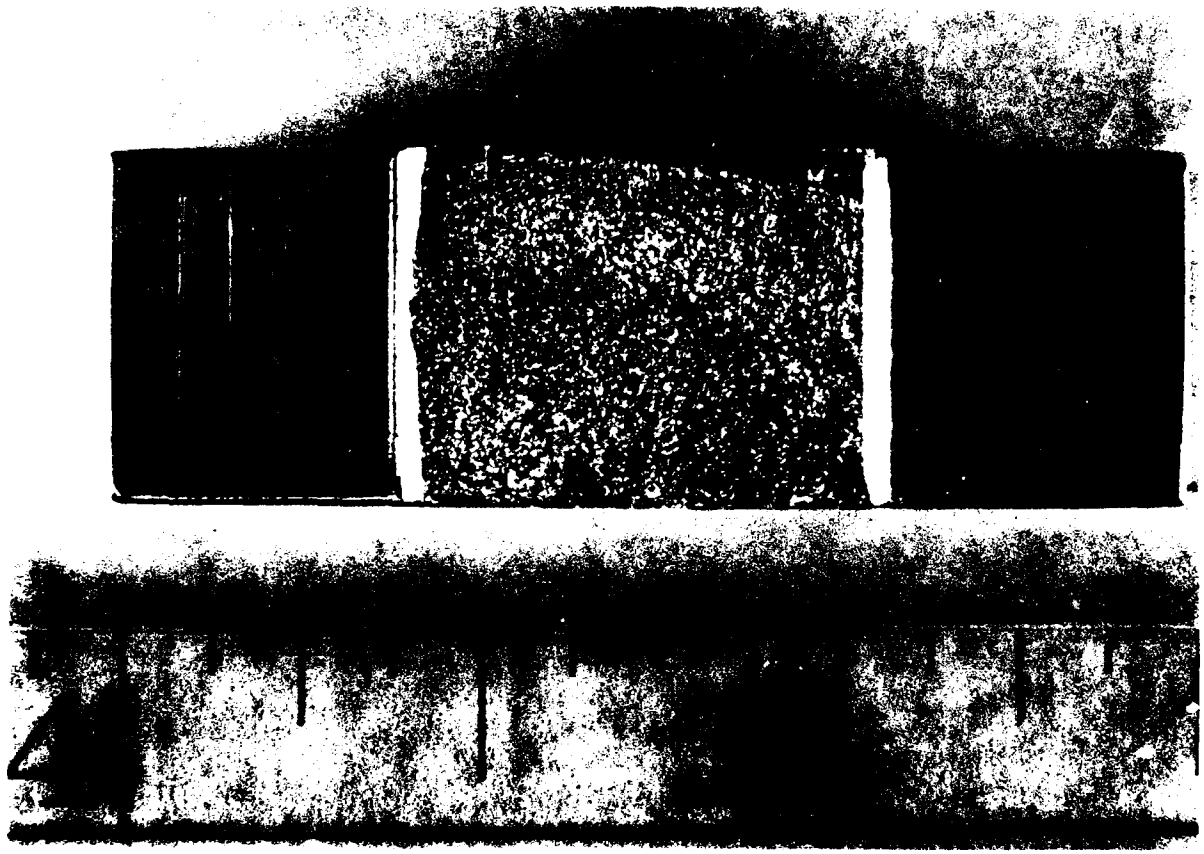

FIGURE 26. FRACTOGRAPH OF SPECIMEN 7 (FIXED PORTION)

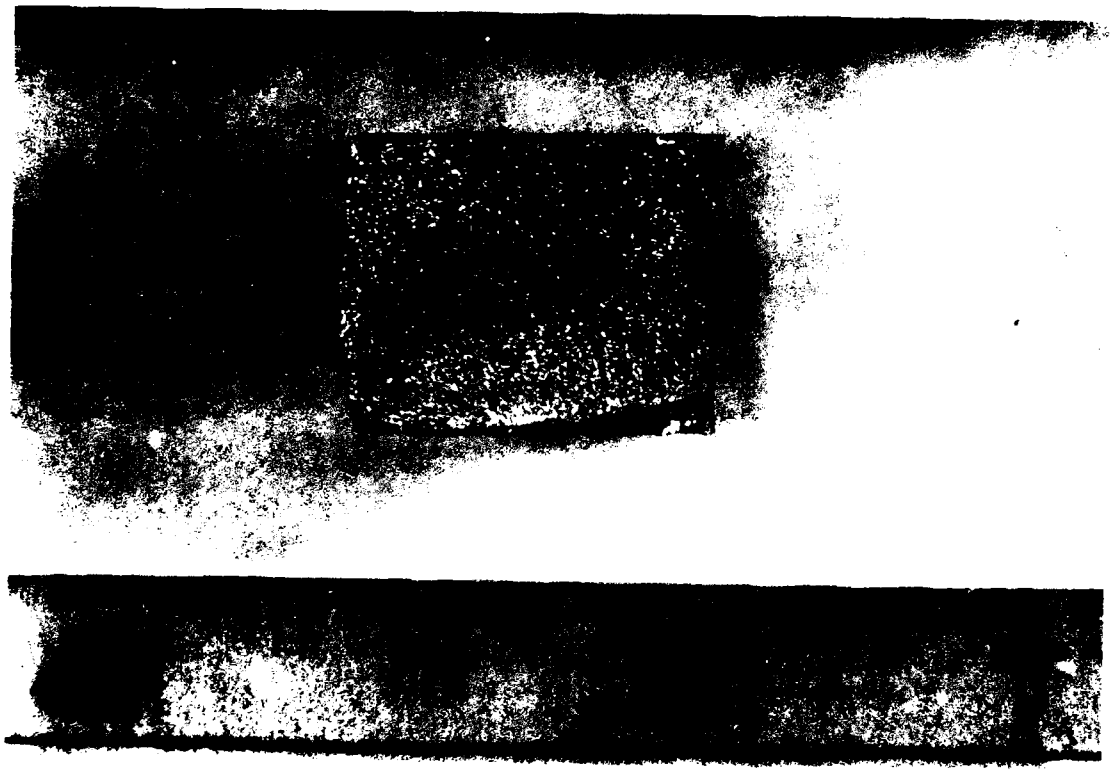

FIGURE 27. FRACTOGRAPH OF SPECIMEN 7 (DRIVEN PORTION)

darkened regions are more widespread in the fractographs of a specimen with an as-received surface condition, Figs. 24 and 25. These regions of the fracture surface are less brittle in nature than the lighter regions, indicating less work hardening. Crack propagation is much slower in such regions than in the lighter, more brittle regions. Another region of interest in the fractographs shown in Figs. 26 and 27 is the very dark region located in one corner of the fracture surface, which indicates that portion of the specimen which underwent ductile flow just prior to specimen fracture.

In addition to fractographs of the fracture surfaces, the cracked surfaces were examined microscopically. Figure 28 shows the transgranular propagation of a fatigue crack in specimen 13. The elongated grains indicate the rolling direction of the 7075-T651 aluminum alloy, and, as can be seen, the crack initiated and propagated perpendicular to the rolling direction. The effect of nonmetallic inclusions and intermetallic particles on fatigue crack propagation is illustrated in Fig. 29 where the crack is shown to have propagated through two such particles. Also shown in Fig. 29 are several deformation bands (short, straight lines) which are evidence of extensive localized plastic deformation. Figure 30 shows a fractured particle which was in the path of the propagating fatigue crack. Both Figs. 29 and 31 demonstrate the presence of secondary cracking. Figure 32 shows a stepped portion of a fatigue crack in specimen 13. The stepped nature of the crack suggests that the crack followed the localized deformation bands during propagation.

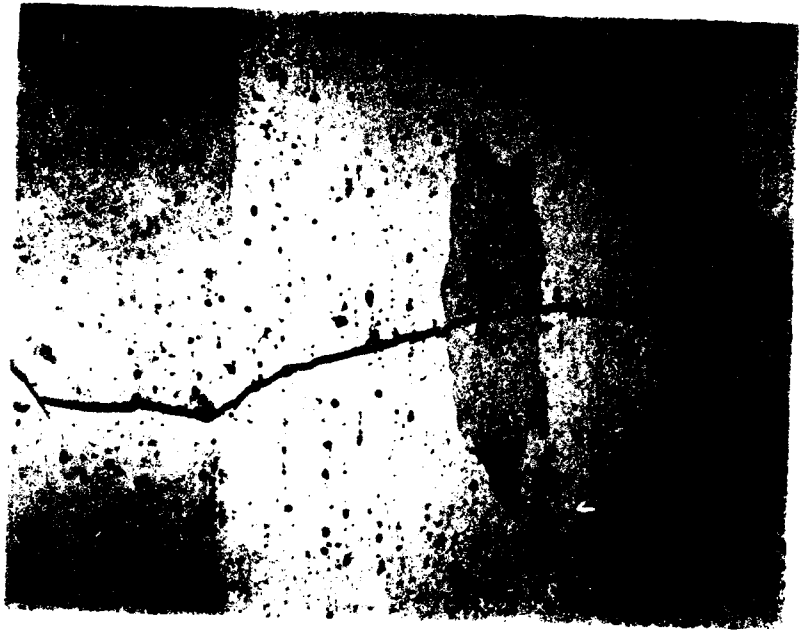

FIGURE 28. PHOTOMICROGRAPH OF CRACK IN SPECIMEN 13 (70 x)

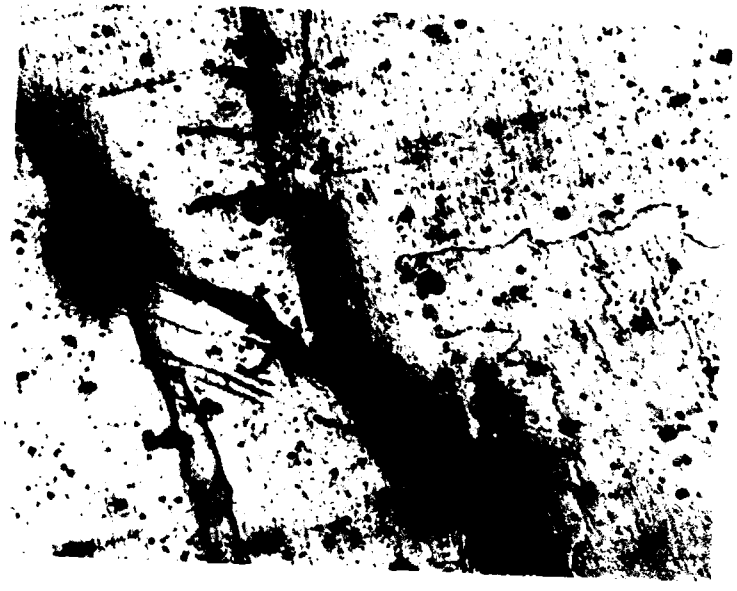

FIGURE 29. PHOTOMICROGRAPH OF SPECIMEN 11 (275 x)

FIGURE 31. PHOTOMICROGRAPH OF SQUARE-CORNERED SPECIMEN (75 x)

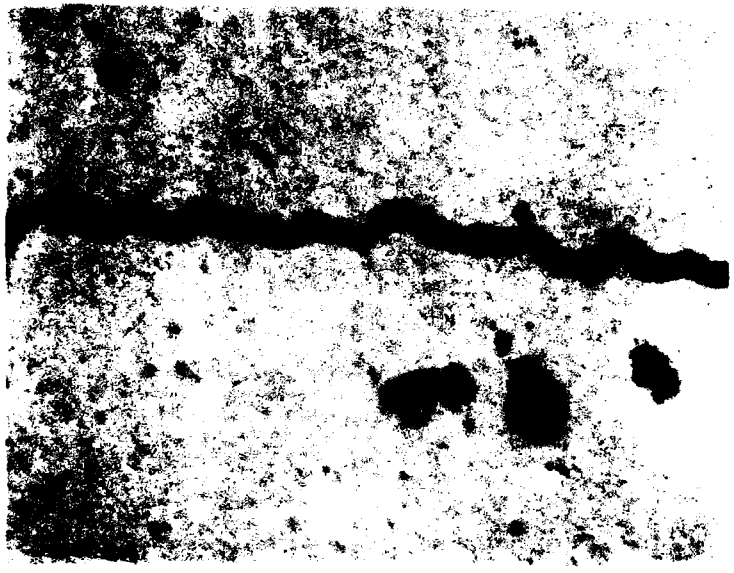

FIGURE 32. PHOTOMICROGRAPH OF SPECIMEN 13 (1500 x)

REPORTS, PUBLICATIONS, PAPERS DELIVERED

1. Duke, John C., Jr., "Simultaneous Acoustic Emission and Ultrasonic Attenuation Monitoring of the Mechanical Deformation of Aluminum," Master's Essay, Department of Mechanics and Materials Science, The Johns Hopkins University, Baltimore, Maryland (1976).

2. Duke, John C., Jr., and Green, Robert E., Jr., "Simultaneous Acoustic Emission and Ultrasonic Attenuation Monitoring of the Mechanical Deformation of Aluminum," Talk presented and paper published in the Proceedings of the Second International Conference on Mechanical Behavior of Materials, Boston, Mass., pp. 1646-1650 (August 1976).

3. Duke, John C., Jr., "Acoustic Emission in 7075 Aluminum," Talk presented at Acoustic Emission Working Group Meeting, Williamsburg, Virginia (October 1976).

4. Kline, Ronald A., "The Acoustic Emission Behavior of Lead-Tin Alloy," Talk presented at Acoustic Emission Working Group Meeting, Williamsburg, Virginia (October 1976).

5. Green, Robert E., Jr., and Pond, Robert B., Sr., "Ultrasonic Detection of Fatigue Damage in Aircraft Components," Annual Report (1976-77), Air Force Office of Scientific Research AFOSR-TR-77-0658 (1977).

6. Green, Robert E., Jr., "Acoustic Emission: A Critical Comparison Between Theory and Experiment," Talk presented and paper published in Proceedings of the Ultrasonics International 1977 Conference, Brighton, England, (June 1977) pp. 235-244, IPC Science and Technology Press Ltd., Guildford, England (1977).

7. Mignogna, Richard B., Duke, John C., Jr., and Green, Robert E., Jr., "Early Detection of Fatigue Cracks in Aircraft Aluminum Alloy Sheets," Talk presented at National Fall Meeting of ASNT, Detroit (October 1977). Submitted for publication in Materials Evaluation.

8. Duke, John C., Jr., and Green, Robert E., Jr., "Simultaneous Monitoring of Acoustic Emission and Ultrasonic Attenuation During Fatigue of 7075 Aluminum," Talk presented at National Spring Meeting of ASNT, New Orleans (April 1977). Accepted for publication in International Journal of Fatigue.

9. Duke, John C., Jr., "Nondestructive Investigation of the Mechanical Deformation of 7075 Aluminum," Ph.D. Dissertation, Department of Mechanics and Materials Science, The Johns Hopkins University, Baltimore, Maryland (1978).

10. Green, Robert E., Jr. and Pond, Robert B., Sr., "Ultrasonic and Acoustic Emission Detection of Fatigue Damage", Annual Report (1977-78), Air Force Office of Scientific Research AFOSR-TR-78-1284 (1978).

11. Duke, John C., Jr., and Green, Robert E., Jr., "Capability of Determining Fatigue Mechanisms in 7075 Aluminum by Combining Ultrasonic Attenuation and Acoustic Emission Monitoring," Paper presented and published in Proceedings of ARPA/AFML Review of Progress in Quantitative NDE Meeting, La Jolla, California (July 1978), AFML-TR-78-205 (January 1979).

12. Green, Robert E., Jr., and Duke, John C., Jr., "Ultrasonic and Acoustic Emission Detection of Fatigue Damage," to be published in Vol. VI International Advances in Nondestructive Testing, Gordon and Breach, New York (1979).

13. Green, Robert E., Jr., "Non-Destructive Methods for the Early Detection of Fatigue Damage in Aircraft Components," Lecture Series No. 103 Non-Destructive Inspection Methods for Propulsion Systems and Components, London, England and Milan, Italy (April 1979), AGARD-LS-103 (1979).

PROFESSIONAL PERSONNEL

In addition to the Principal Investigators, Professor Robert E. Green, Jr., and Professor Robert B. Pond, Sr., the following persons have been engaged with various aspects of the research program during the past year:

Dr. John C. Duke, Jr. (Postdoctoral Research Associate)

Dr. Steven E. Fick (Postdoctoral Research Associate)

Mr. B. Boro Djordjevic (Graduate Student)

Mr. Carl Lee Friant (Graduate Student)

Mr. Sanford R. Buxbaum (Graduate Student)